Chapter 2

Paleoclimatic Ocean Circulation and Sea-Level Changes

Stefan Rahmstorf and Georg Feulner
Potsdam Institute for Climate Impact Research, Potsdam, Germany

Chapter Outline

1. INTRODUCTION

The oceans have been an important factor in shaping Earth's past climate. Their circulation has influenced the overlying atmosphere (see, e.g., reviews of Alley et al., 2002; Clark et al., 2002; Rahmstorf, 2002) and they have acted, as they still do, as a repository for heat and gases. One consequence of the ocean's response to climate change, which is acutely important for human society, is sea-level change (the book *Understanding sea-level rise and variability* edited by Church et al., 2010 gives an excellent overview of this topic; see Chapter 27). This chapter provides a brief introductory discussion of past ocean circulation and sea-level changes before the time of instrumental measurements.

We describe the methods used for reconstructing past ocean states using proxy data and models and give specific examples of ocean circulation and sea-level changes in Earth's history. This is a large field with a vast body of scientific literature, thanks to a great research community with many excellent scholars, and this chapter can certainly not provide a comprehensive review. Rather, we provide the reader with an introduction to some of the main methods, together with examples of the research questions being addressed. Inevitably, the choice of examples is to some extent subjective and dependent on the authors' areas of expertise. However, we hope to provide a basis of understanding this exciting and important topic in which many puzzles still wait to be solved.

The dominant drivers of paleoclimatic change depend on the timescale considered. Two important ones are tectonic and orbital timescales (Ruddiman, 2000). The former covers climatic changes on timescales of some millions of years up to the age of the Earth of 4.6 billion years. These changes are driven by tectonic processes associated with the solid Earth's internal heat, but also include the evolution of life which has altered the composition of Earth's atmosphere (Stanley, 2005). Plate tectonics are a key driver of Earth's long-term carbon cycle which controls atmospheric CO_2 concentration on multimillion year timescales by exchanging carbon with the Earth's crust. Plate tectonics also alter the Earth's geography with effects on climate, that

Ocean Circulation and Climate, Vol. 103. http://dx.doi.org/10.1016/B978-0-12-391851-2.00002-7

is, the position of continents and oceans, the formation of mountain ranges, and the opening or closing of ocean gateways.

On timescales of thousands to hundreds of thousands of years, the Earth's orbital cycles are an important (probably dominant) driver of climate changes. These Milankovitch cycles (Milankovitch, 1941) have main periods of 23,000 years (precession), 41,000 years (tilt of Earth's axis), and ~100,000 as well as ~400,000 years (eccentricity of Earth's orbit) and have a strong effect on the seasonal and latitudinal distribution of solar radiation (Ruddiman, 2000). These orbital cycles are pacemakers of the Quaternary glaciations (see Section 3).

In addition, climate has been changed by variability in the sun's radiation output and by internal processes in the climate system, such as through instabilities in ocean circulation or ice sheets. It is important to distinguish between changes in global-mean temperature (primarily dependent on Earth's global radiation balance but with small transient variations due to changes in ocean heat storage; Chapter 27) and those climate changes caused by redistribution of heat such as through changing oceanic or atmospheric heat transport (Chapter 29).

2. RECONSTRUCTING PAST OCEAN STATES

Past changes in ocean circulation and sea level have left a number of lasting records that can still be sampled today, for example, in the form of sediments on the ocean floor, uplifted marine terraces, or ancient corals. In order to interpret these proxy data and to provide quantitatively consistent scenarios of past ocean states and changes, a range of models is used. The combination of proxy data and models allows us to formulate and test hypotheses about mechanisms of past ocean and climate changes.

2.1. Proxies for Past Ocean Circulation

Although there are numerous sources of information about past ocean states in the sedimentary record, it is not easy to interpret this information in terms of specific changes in ocean circulation. In fact, this is an inverse problem where the products of a given ocean circulation (in terms of sediment deposition) are used to infer what the ocean circulation state may have been. Solving this inverse problem is complicated by the fact that what is found in the sedimentary record is usually the result of multiple influencing factors, the data have uncertainties both in dating and in the parameter values measured, and their time resolution is often seriously limited (e.g., by bioturbation of the sediment) so that they need to be interpreted as some kind of time average.

Tracers of past ocean circulation can be broadly grouped into three types: nutrient-type water mass tracers, conservative water mass tracers, and circulation rate tracers. In addition, special cases are the neodymium isotope ratios and nongeochemical tracers. An excellent, much more detailed review along these lines is found in Lynch-Stieglitz (2003); see also Chapter 26.

2.1.1. Nutrient Water Mass Tracers

Nutrient water mass tracers are those elements that are involved in biological activity and thus behave like nutrients, that is, like the key constituents of marine organic matter: carbon, nitrogen, and phosphorus. These are taken up by marine life during primary production near the ocean surface and hence tend to be depleted in surface waters. In many parts of the ocean, nitrogen or phosphorus are close to zero concentration at the surface since their availability is the limiting factor of primary production (these are *biolimiting elements*). As dead organic matter sinks through the water column and decays there or on the seafloor, nutrients are returned to the water. Thus, water masses typically gain in nutrient concentration over time after they have left the surface ocean. In the present-day Atlantic, the main water masses of Antarctic Intermediate Water (AAIW), North Atlantic Deep Water (NADW), and Antarctic Bottom Water (AABW) reflect the initial nutrient content set by the respective surface value in the water mass formation region and by subsequent mixing between these water masses. In the deep Pacific Ocean, nutrient content reflects the initial value of the inflowing AABW, progressively increasing as the water mass ages along the pathway that it spreads.

The basic principle behind the use of nutrient-style watermass tracers is to use elements (or isotopes of elements) that behave like nutrients but that are preserved in sediments (typically in the calcium carbonate shells of bottom dwelling marine organisms such as foraminifera), so that their distribution during past epochs can be mapped using a large number of sediment cores from different ocean depths. Prominent among these tracers are carbon isotope ratios ($\delta^{13}C$) (Deuser and Hunt, 1969) and the cadmium/calcium ratio (Cd/Ca) (Boyle et al., 1976).

A basic precondition for using the composition of shells (or "tests") of marine organisms as water mass indicators is that the chemical composition of these shells faithfully reflects that of the seawater they grew in. This is illustrated for two species of foraminifera in Figure 2.1 for their carbon isotope ratios.

The choice of species is important: not all are as well suited as the two shown. Biological processes can lead to preferential uptake of the lighter ^{12}C as compared to ^{13}C, so that a systematic offset arises between $\delta^{13}C$ (a measure of relative ^{13}C content) in the shells relative to the ambient

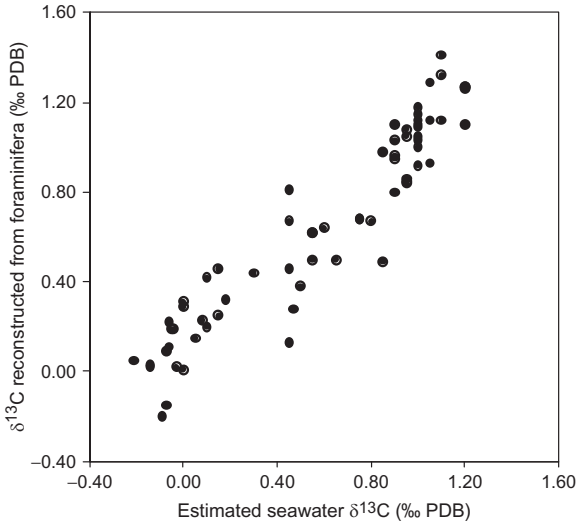

FIGURE 2.1 Carbon isotopic composition of core top benthic foraminifera in the genera *Cibicidoides* and *Planulina* versus estimated carbon isotopic composition of dissolved inorganic carbon in the water column above core location. *From Lynch-Stieglitz (2003) after Duplessy et al. (1984).*

water (Wefer and Berger, 1991). This is generally the case for planktonic foraminifera (i.e., those living in the water column), which thus do not record water mass properties as well as the benthic (i.e., bottom dwelling) species shown in Figure 2.1 (Spero and Lea, 1996). Hence, benthic foraminifera are commonly used to reconstruct past deepwater masses. Within benthic foraminifera, differences between species are thought to mainly arise because of their different choices of microhabitat (e.g., Tachikawa and Elderfield, 2002). Some (e.g., *Uvigerina*) live not on the surface of the sediments but within the pore water, which is depleted in $\delta^{13}C$ relative to the bottom water. This example highlights that much experience and a detailed understanding of the processes is required in order to arrive at robust conclusions from proxy data; it takes considerable time and detective work to develop proxies to the level where they can be properly interpreted.

The Cd/Ca ratio in shells of benthic foraminifera is another commonly used proxy for nutrient cycling in the ocean, because these elements are incorporated in the shells in proportion to their abundance in the water. However, there is a depth-dependent empirical factor that needs to be accounted for in reconstructing seawater cadmium concentrations from the shells (Boyle, 1992).

Cadmium in seawater is distributed much like major nutrients (e.g., phosphorus)—indeed it shows an almost linear relationship to phosphorus. Apparently, marine plankton metabolize cadmium like a nutrient, so it is depleted in warm surface waters where primary productivity occurs and enriched in deepwaters where organic matter decays (Boyle et al., 1976). A complication that needs to be considered in the interpretation is that the biological relation between cadmium and phosphorus is not exactly linear due to preferential uptake, so that a curved P versus Cd relation is expected along a water mass that is progressively nutrient-depleted by biological activity (Elderfield and Rickaby, 2000). In contrast, a straight mixing line would be obtained by progressive mixing of two distinct water masses with low and high nutrient content.

Further nutrient-style tracers include barium and zinc, measured as Ba/Ca and Zn/Ca ratios, respectively (Lynch-Stieglitz, 2003).

2.1.2. Conservative Water Mass Tracers

Conservative water mass tracers are those that (in contrast to nutrients) have no sources or sinks in the subsurface ocean, so that their properties are set at the ocean surface and the variations deeper in the water column reflect the transport and mixing of water masses (see Chapters 6–8 and 26). This is the case with temperature and salinity, the standard water mass tracers of modern physical oceanography. Such a conservative tracer is magnesium, as the Mg/Ca ratio in benthic foraminifera reflects the water temperature during calcification, that is, that in which the organisms lived (Rosenthal et al., 1997). The major challenge here is to determine the water temperature from Mg/Ca with sufficient accuracy in order to reconstruct the relatively small gradients in deepwater temperatures.

Another common conservative tracer is the oxygen isotope ratio, expressed as $\delta^{18}O$ (i.e., the relative deviation of ^{18}O content from a standard). The $\delta^{18}O$ value of ocean water is set at the surface depending on water exchange (e.g., by evaporation and precipitation), hence it is closely linked to salinity (Lynch-Stieglitz, 2003). Since ^{18}O is heavier than the common ^{16}O, it evaporates less easily. Therefore, continental ice (made from snow) is depleted in ^{18}O and the formation of large ice sheets leads to a sizeable increase in ^{18}O in ocean water. During the last glacial maximum (LGM), sea level was $\sim$130 m lower than today; the missing water was ^{18}O depleted and stored on land in the form of ice. The remaining water therefore was proportionally ^{18}O enriched by about 1‰ in $\delta^{18}O$. In fact, this glacial ^{18}O peak can still be found today in the pore water of sediments formed at the time, now typically found at a depth of 20–60 m within the sediments, depending on location (Schrag et al., 2002).

The $\delta^{18}O$ in the calcite shells of foraminifera depends on that of the surrounding waters and on the temperature (there is a temperature-dependent biological fractionation) (e.g., Duplessy et al., 2002). Hence, if the $\delta^{18}O$ of the water or the salinity and ice volume effect is known (or negligible), $\delta^{18}O$ in these shells can be used as a proxy for local temperature (Figure 2.2). The slope shown there suggests that

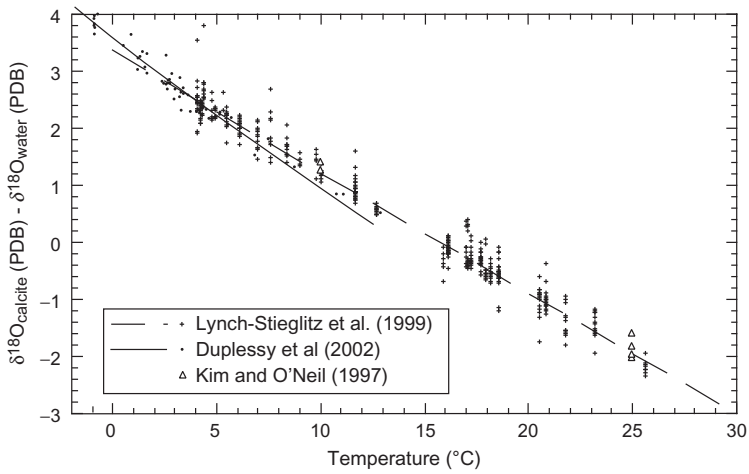

FIGURE 2.2 The isotopic fractionation, expressed as the difference between the $\delta^{18}O$ of foraminiferal calcite and the $\delta^{18}O$ of seawater versus temperature of calcification. Cibicidoides and Planulina from Lynch-Stieglitz et al. (1999) (—+) and Duplessy et al. (2002) (—•) are shown along with the inorganic precipitation experiments of Kim and O'Neil (1997) (Δ). *From Lynch-Stieglitz (2003).*

benthic $\delta^{18}O$ in calcite increases by ~0.25‰ per °C. However, $\delta^{18}O$ is useful as a water mass tracer even if the effects of temperature and salinity cannot be separated, since they are both conservative tracers (Lynch-Stieglitz, 2003).

2.1.3. Circulation Rate Tracers

The tracers discussed so far provide information on the water masses present in the past at locations for which we have sediment data, including on the relative contribution of waters from different source regions and thus relative renewal rates. But they do not reveal the rates of ocean circulation. Various methods have been applied to estimate rates.

One set of techniques uses radiocarbon (^{14}C), which is created in the atmosphere due to cosmic rays. While the surface ocean is close to equilibrium with atmospheric radiocarbon content, this decays below the surface according to the half-life of ^{14}C of 5730 years. In the modern ocean, this is a very useful measure of the age of water masses, that is, the time elapsed since they left the surface (Stuiver et al., 1983).

The problem with using ^{14}C in paleoclimatic studies is that it continues to decay after it is incorporated in calcite shells, so that the time recorded by ^{14}C ages of benthic foraminifera is the age of the deepwater plus the age of the foraminifera shell. To derive the deepwater age, an independent measure of the shell age is needed. This can be derived from the age of planktonic foraminifera collocated in the same sediment (Broecker et al., 1988). Or the method is applied to benthic corals, which can be dated independently using uranium dating (Adkins et al., 1998).

Another approach is measuring the ratio of protactinium to thorium, $^{231}Pa/^{230}Th$. These elements are created uniformly throughout the water column by uranium decay and rapidly removed into the sediments by reacting with sinking marine particles (Anderson et al., 1983). Since the efficiency with which both elements are removed is different, their ratio depends on how long this removal process has operated, for example, along the path of NADW flowing south in the Atlantic. This method has been used to infer NADW flow rates during the LGM (Yu et al., 1996). However, this ratio is also sensitive to particle fluxes and composition and interpretation is not straightforward.

Finally, the geostrophic method, a standard approach in physical oceanography, can also be applied to paleoclimate. It requires knowledge of density profiles in the past upper ocean, which can be estimated from $\delta^{18}O$ in benthic foraminifera (see Section 2.1.2). This method has been used to reconstruct past Gulf Stream flow in the Florida Straits (Lynch-Stieglitz et al., 1999). To reconstruct density profiles, benthic foraminifera are required from different depth levels and thus a range of cores from different water depths.

2.1.4. Other Tracers

Some other tracers exist, that neither behave like nutrients (i.e., with biological sources and sinks) nor are conservative. An example is neodymium isotopes, which have sources and sinks at the ocean–sediment interface, because neodymium precipitates in metallic crusts or is mobilized from detrital material. This gives water masses like NADW a distinctive neodymium isotope signature that can be used to assess the mixing of water masses of different origin (Rutberg et al., 2000).

2.2. Past Sea-Level Proxies

When studying sea level, we first need to distinguish relative from absolute sea-level changes. Absolute sea-level changes are changes in the sea surface height with respect

to a fixed absolute reference frame, for example, the center of the Earth, as measured from a satellite. Relative sea-level change is what an observer (or tide gauge) at the coast would have experienced. It is measured locally, relative to the land and is thus the sum of absolute sea-level changes and vertical motions of the land. In the recent geological past (last ~4000 years), vertical land motion was the dominant factor of relative sea-level change on many coastlines.

Within absolute sea-level changes, it is useful to distinguish local from global changes. There are mechanisms (e.g., a change in wind regime) that can change sea level locally without having any effect on global-mean water volume and sea level. Changes in global-mean (or eustatic) sea level consist of changes in the volume of seawater (arising either from mean density changes or from addition of water, e.g., from melting continental ice) and of changes in the volume of the ocean basins that contain it (due to plate tectonics or isostatic adjustment).

Past sea-level changes are reconstructed using sea-level indicators (proxies) that have a specific (and known) relationship to sea level. A sea-level indicator is any biological, chemical, or physical proxy that can be reliably related to sea level. These include relic beaches, ancient corals, intertidal sediment, and historic human structures built at or close to contemporary sea level (e.g., fish ponds, ports, or coastal wells). The relationship between a proxy and sea level is established from modern, observable examples. When a fossil example of the sea-level indicator is located, it is dated and interpreted based on its modern counterparts. The resulting reconstruction estimates the unique position in time and space of former sea level as a sea-level index point. Compilations of index points allow patterns and trends in relative sea level to be described. Almost all of these record the local sea level relative to the land, and a major challenge in interpreting these data is to disentangle the land motions from true sea-level changes, and to obtain a reconstruction of global sea-level history that can be linked to climate. More detailed reviews are found, for example, in Lambeck et al. (2010) and Shennan et al. (2007).

2.2.1. Coastal Morphology and Corals

Waves, tides, sediment transport, or reef-building corals shape the coastline, and in some places, the resulting coastal land forms are found today at elevations far away from present-day sea level. Tidal notches that have been eroded out of coastal cliffs during extended periods of stable sea level can today be seen at different elevations (Pirazzoli and Evelpidou, 2013). Marine terraces form when the flat former beach front is uplifted or inundated. The sequence of reef terraces on Huon Peninsula (Papua New Guinea) is famous: the reef front from the last interglacial has been uplifted over 100 m above the present sea level due to seismic activity (Figure 2.3; McCulloch et al., 1999; Ota and Chappell, 1999). For large relative sea-level changes, these are useful indicators.

Since corals can grow tens of meters below the water surface but not above it, the envelope of (radiometrically dated) ancient corals can provide a lower limit to past relative sea level (e.g., Lambeck, 2002). Most useful are coral species that have a particularly close relation to sea level, such as Elkhorn coral (Acropora palmata). Coral microatolls are disc-shaped coral colonies that have been stopped from further upward growth by exposure at low tides, so that the center of the upper surface is dead and coral growth occurs laterally around the margin (Figure 2.4; Woodroffe and McLean, 1990). Because corals show annual growth bands, precise dating is possible, and microatolls can reveal interannual to decadal sea-level changes of the order of ±5 cm and millennial changes of the order of ±25 cm (Lambeck et al., 2010). However, since they

FIGURE 2.3 Uplifted coral reef terraces of the Huon Peninsula, Papua New Guinea. In this area, the land is moving upward at a rate of ~2 m/1000 years. Consequently, fringing coral reefs along the coast get uplifted. These ancient reefs now form a succession of "steps," or terraces, in the coastal landscape, with the youngest reefs closest to the coast, and the oldest reefs at higher elevation further back from the coast. The oldest reefs in this image are about 250,000 years old and are seen as terraces toward the top-left of the photo. *Photo: Sandy Tudhope.*

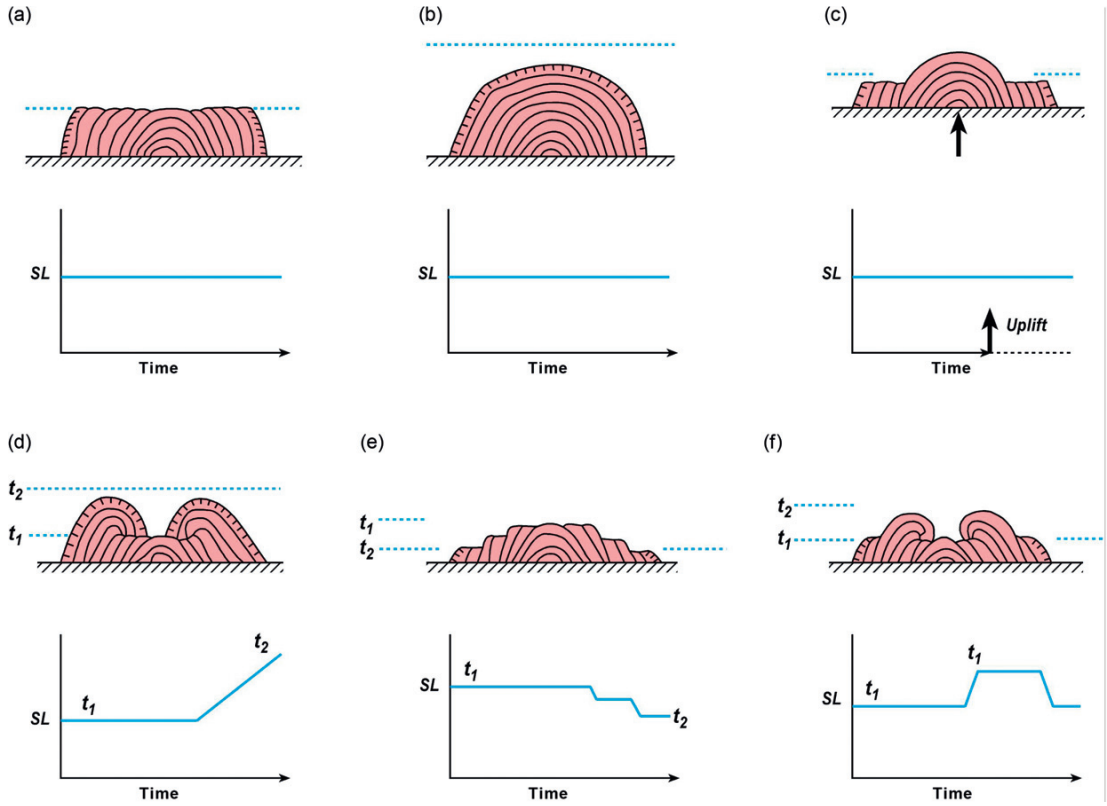

FIGURE 2.4 Schematic illustration of the response of coral, particularly the upper surface of microatolls, to changes of sea level or uplift of the land, as shown by annual banding within the coral skeleton. (a) If sea level (SL) remains constant from year to year, a massive coral that has grown up to sea level continues to grow outward but with its upper surface constrained at water level. The inner part of the upper surface is partly protected by the outer rim, which will usually be the only living part of the colony. (b) If the coral does not reach water level, it adopts a domed growth form and is not constrained by water level. Its upper surface could be several meters below sea level. (c) If the coast undergoes uplift (or sea level falls), a coral previously not limited by sea level may be raised above its growth limit and the exposed upper surface will die, but with continued lateral growth at a lower elevation. (d) If the water level increases, a coral previously constrained by exposure at low tides can resume vertical growth and begin to overgrow the formerly dead upper surface. (e) If water level falls episodically, then the microatoll adopts the form of a series of terracettes. (f) If there are fluctuations of water level with a periodicity of several years then the upper surface of the microatoll consists of a series of concentric undulations. Such a pattern can be seen on microatolls from reef flats in the central Pacific where El Niño results in interannual variations in sea level. *Reproduced from Lambeck et al. (2010).*

mainly record how low the water drops at low tide, highly localized events (such as storms) that change the shoreline and affect tidal flow and the formation of pools on reef flats can alter the results. As with most proxy data, it is the combination of data from different sites and/or using different methods that ultimately provides robust results.

2.2.2. Sediment Cores

Sheltered, low-energy coasts are often vegetated by salt marshes in temperate climate zones and mangroves in the tropics. The distribution of these ecosystems is fundamentally and intrinsically tied to tidal limits and sea level. Under regimes of rising relative sea level, organic and muddy sediment is deposited in these environments. Over time the sediment accumulates to form an important archive from which relative sea level can be reconstructed. The sediment is dated using the radiometric method (principally radiocarbon), while sea-level indicators preserved in the sediment such as identifiable plants, diatoms, and foraminifera are used to determine the vertical location of the marsh surface at any time relative to the tidal range (Scott and Medioli, 1978). Since the current vertical position of the sediment is used in reconstructing the past sea level, an important issue is that no compaction of the sediment has occurred after it has formed (Allen, 2000). The procedure is illustrated in Figure 2.5. This method is useful for high-resolution reconstruction of sea-level changes over the last few millennia, with a vertical precision of ±5–20 cm (e.g., Gehrels, 1994; Donnelly et al., 2004; Kemp et al., 2011).

A notable exception to the usual records of local relative sea level is the $\delta^{18}O$ in benthic foraminifera, which depends

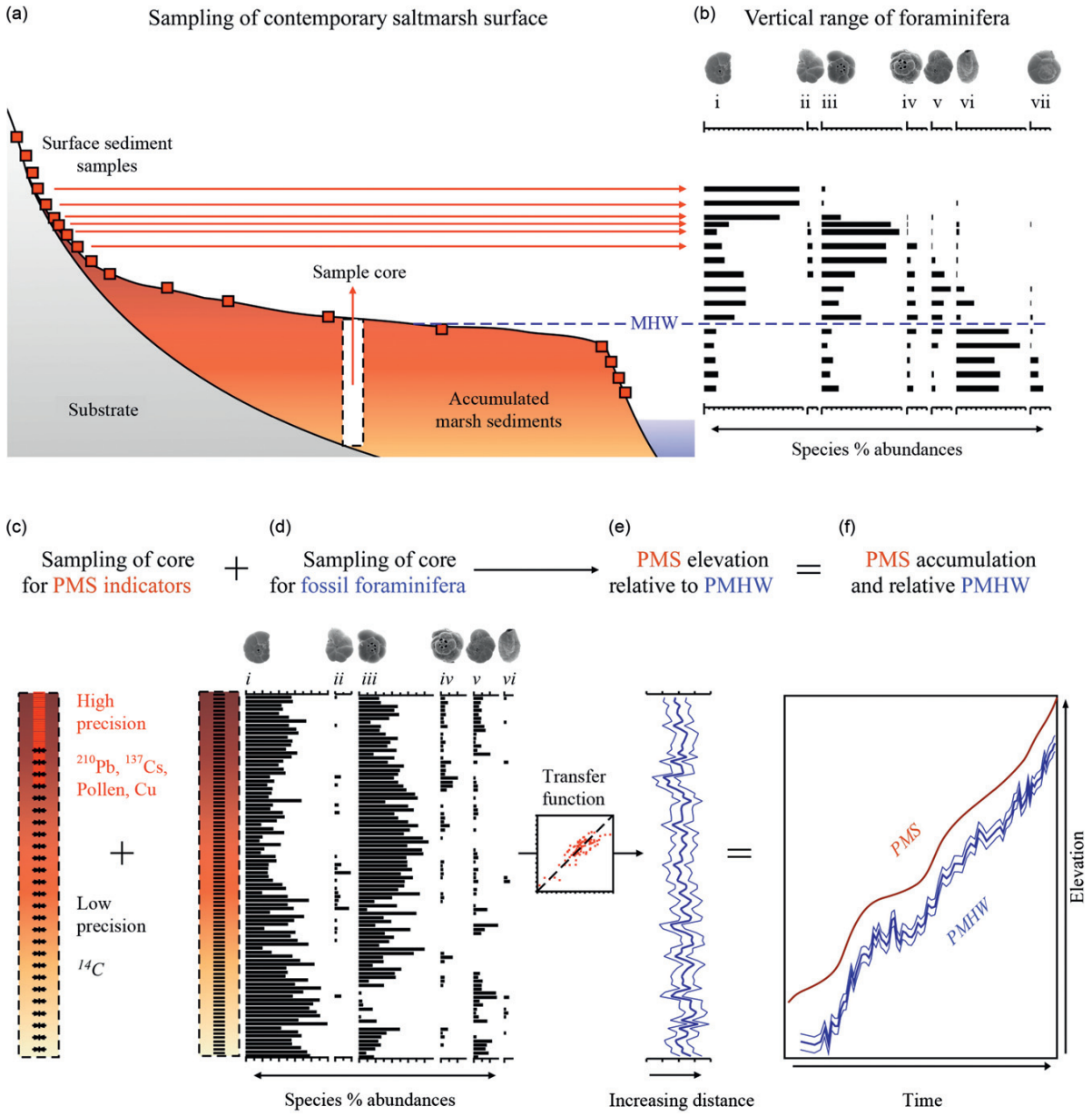

FIGURE 2.5 Schematic illustration of the steps involved in reconstructing sea-level changes using salt marsh microfossils. The contemporary surface distribution (a) of foraminifera species (b) is related to elevation of the marsh surface above a tidal datum and subsequently represented by a transfer function. Paleo-marsh surface (PMS) indicators are sampled in a sediment core (c), with dating control provided by radiometric techniques. The core is also analyzed for fossil foraminifera species abundances (d), which are interpreted in terms of PMS height (e) relative to paleo-mean high water (PMHW) using the transfer function arrived on the basis of steps (a) and (b). These combine (f) to reconstruct the PMS accumulation history and rate of relative sea-level rise. *Reproduced from Lambeck et al. (2010).*

on the total ice volume on land (see Section 2.1.2). Since ice volume changes are by far the dominant cause of global sea-level changes during glacial–interglacial cycles, $\delta^{18}O$ is a very useful global sea-level tracer on these timescales (Waelbroeck et al., 2002).

2.2.3. *Manmade Sea-Level Indicators*

Ancient buildings or artifacts and their relation to sea level can provide clues about past sea-level changes. The oldest example is the famous cave paintings of Cosquer cave in

southern France from the last ice age (from 19 to 27 kyears BP); today the entrance of the then inhabited cave is 37 m below the sea surface (Lambeck and Bard, 2000). Ancient wells submerged off the coast of Israel have been dated to be between 8200- and 9500-years old (Sivan et al., 2004). Only divers can today visit the sunken city of Baia in Italy to marvel at the floor mosaics (Passaro et al., 2013).

More useful as a sea-level constraint are structures with a precise relation to sea level, such as ancient harbor walls or the Roman fish tanks which were connected to the sea with a series of canals and sluice gates for water exchange, which constrain the sea level at the time these ponds were built to within a narrow range (Lambeck et al., 2004). Remains of the Roman market at Pozzuoli include pillars that have borings by marine organisms up to 7 m above present-day sea level; the site must have been submerged up to that level and uplifted again between the time it was built and the present (due to volcanic activity). Remarkably, already in 1832, Lyell showed this in his *Principles of Geology* (Lyell, 1832). More recently, old paintings of Venice have been analyzed for the level up to which the palace walls are covered by brown algae (Camuffo and Sturaro, 2003; Figure 2.6). Canaletto and his students painted these palaces along the canals with great accuracy using a *camera obscura*. Results show a ~70-cm relative sea-level rise since the first half of the eighteenth century (mostly due to land subsidence) which is the main cause of the frequent floodings of Venice today (Carbognin et al., 2010).

2.3. Models

In principle, the full range of ocean models described elsewhere in this book can also be applied to paleoclimate. The major difficulties are the specification of paleoclimatic boundary conditions and computational cost. Computing a very different ocean circulation, like that of the LGM, requires millennia of model time until a new thermodynamic equilibrium of the circulation with the temperature and salinity fields is reached.

Ocean-only models require boundary conditions for the entire ocean surface, a demand that is very difficult to satisfy. Historically, ocean-only models have often been driven by prescribing surface temperatures and salinities using a relaxation boundary condition and prescribed wind forcing anomalies (e.g., Fichefet et al., 1994). But even if a global map of these quantities is available, fundamental problems with relaxation boundary conditions remain: if the surface temperature and salinity fields in the model perfectly match the data, then the heat and freshwater fluxes vanish, but if the fluxes are correct, then errors in temperature and salinity must exist. Hence relaxation boundary conditions cannot converge to the "true" solution but only approximate it in a first-order sense.

High-resolution (eddy-permitting) ocean models are starting to be applied to paleoclimatic studies (Ballarotta et al., 2013), but due to computational cost, these models typically can only be run for a limited time period of the order of decades, which means they remain close to the initial conditions for temperature and salinity in the water column and essentially diagnose a velocity field that is dynamically consistent with this initial distribution.

Coupled ocean–atmosphere models are best suited for paleoclimatic applications (Braconnot et al., 2007a,b) because they can simulate the surface climate together with atmospheric and oceanic circulations in a physically consistent

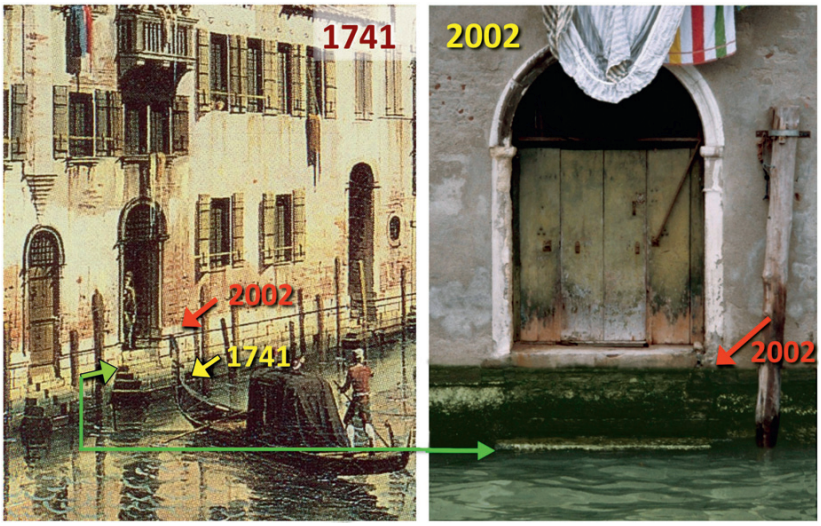

FIGURE 2.6 Left: A detail from B. Bellotto's painting S. Giovanni e Paolo (1741). The two arrows give the level of the algae belt in 1741 (lower) and today (upper) as derived from on-site observations. The painting shows that there were two front steps above the green belt. The displacement is 77 ± 10 cm. Right: The same door today. The picture was taken during low tide and the top step of the old front stairs is just visible (green arrow). The door was walled up with bricks in the first 70 cm above the front step to avoid water penetration. *From Camuffo and Sturaro (2003).*

way, including the air–sea fluxes which are crucial in driving the ocean circulation. The boundary conditions required are less demanding. For example, for a simulation of the LGM, besides the orbital parameters, one needs the atmospheric composition (greenhouse gases, dust load) and specification of the land surface (vegetation and ice cover). More comprehensive Earth system models require increasingly fewer external boundary conditions as more processes are included in the simulation. If an ice sheet model is included, then the ice sheet configuration need not be prescribed; if a vegetation model is included, then the vegetation cover is likewise predicted rather than prescribed, and with a closed carbon cycle the atmospheric CO_2 concentration is also predicted by the model. Only the latter approach can ultimately explain glacial cycles—as long as prescribed CO_2 is still included, the forcing already includes the same sawtooth-shaped 100-kyear cycles as the climate response, so even a simple linear model can produce reasonable glacial cycles. But the Milankovitch forcing—the ultimate external driver of the glacial cycles—does not resemble the climate response, so that obtaining realistic glacial cycles only from this forcing requires capturing the key nonlinearities in the climate system.

When going back deeper into Earth's geologic past, boundary conditions such as the atmospheric greenhouse gas content are increasingly poorly known, and the additional problem arises that the ocean's bottom topography also becomes more and more uncertain due to the action of plate tectonics.

Models of intermediate complexity (Claussen et al., 2002) are particularly suited for paleoclimate studies, not only because their computational speed allows for the long simulated time periods needed in paleoclimate experiments (e.g., related to the slow time scale of ice sheet formation), but also because modeling such a complex nonlinear system well outside the realm of experience (i.e., modern climate) is a process of learning by trial and error. Model runs are compared to proxy data, discrepancies are inevitably found, and their physical (or computational) reasons are investigated; on this basis, model improvements are made and the next round of experiments is performed, and so on—this learning process requires a large number of model experiments to reach a mature stage. Full-blown general circulation models, which explicitly simulate weather in the atmosphere with the associated short time steps, typically only allow a few model experiments and thus the first tentative steps in this development and learning process. Also, explicitly resolving synoptic timescales (i.e., weather) may not be needed for most paleoclimatic studies.

In terms of experimental design, historically the first approach was the simulation of time slices, that is, a "snapshot" of a climate state at a particular point (or period) in time, such as the mid-Holocene and the LGM (Braconnot et al., 2007a,b). In this case, a model is driven by boundary conditions that are unchanging in time, and it needs to be run until an equilibrium with these fixed boundary conditions has been reached. More advanced are transient simulations where boundary conditions are changing over time, for example, to simulate climate evolution over a full glacial cycle (Ganopolski et al., 2010). Particularly when boundary conditions are poorly known, sensitivity studies are a useful approach in which a whole range of possibilities is investigated in an ensemble of model runs.

Increasingly, models are used to simulate not just paleo-ocean circulation but also the transport, transformation, and sedimentation processes of particular tracers, so that the models effectively simulate the formation of a sedimentary sequence that can be directly compared to proxy data from sediment cores (Schmidt, 1999; Hesse et al., 2011). This is a promising alternative to comparing a modeled circulation state to one heuristically inferred backward from proxy data. One still would like to draw inferences about past ocean circulation, so the inverse problem remains, but it can be approached in a more quantitative manner with the help of such models, for example, by data assimilation techniques using proxy data.

Modeling sea-level changes in principle require models of all the processes that contribute to sea level. For the large global sea-level changes during glacial cycles, the problem essentially reduces to continental ice sheet modeling, the dominant contribution. The much smaller sea-level variations during the last few millennia, including the twentieth century rise, on the other hand, are caused by a more even mix of thermal expansion and ice sheet and glacier mass changes which are not easily modeled (see Chapter 16). As a complementary approach to these "bottom up" models of individual processes, semiempirical models have been developed, which link global sea level to global-mean temperature or radiative forcing with simple equations calibrated with empirical data (Rahmstorf, 2007; Grinsted et al., 2010). The equation used in a semiempirical model is typically a variation on the idea that the rate of sea-level rise is proportional to the amount of warming above a previous temperature level at which sea level was stable. In some cases (particularly for multicentury timescales), a time scale of the response is explicitly included.

To aid in the interpretation of sea-level proxies, an entirely different class of models is used: those that describe vertical land motions, for example, models of glacial isostatic adjustment (GIA; Argus and Peltier, 2010). This is important to derive absolute sea-level changes from proxy records of relative sea level, by subtracting the local vertical land movement.

3. THE OCEANS IN THE QUATERNARY

The Quaternary period covers roughly the last 2.5 million years, which are characterized by periodic glaciations. A prime target for reconstructions and models of the paleo-ocean has been the LGM about 20 kyears before present, because it is the most recent period with a

massively different climate (so the signal is large). Interglacial climate, full glacial cycles, and millennial-scale events have also been targets of scientific interest, as well as of course the climate evolution of the most recent millennia preceding the twentieth century global warming.

3.1. The Last Glacial Maximum

The LGM is defined as the time period when the continental ice sheets reached their maximum total mass during the last ice age; Clark et al. identify the interval between 26.5 and 19 kyears BP with the LGM (Clark et al., 2009). Maximum ice sheet size coincides with a minimum in global sea level since continental ice mass is by far the dominant factor in glacial–interglacial sea-level changes. Figure 2.7 shows global sea-level history across the LGM based on four proxy records for relative sea level from far-field sites (i.e., sites that are remote from the location of the ice sheets) as well as an independent estimate of eustatic sea-level changes based on a large number of proxy estimates of the size of continental ice masses. Global sea level during the LGM was 120–135 m lower than at present (Peltier and Fairbanks, 2006).

The timing of the LGM coincides with a strong minimum in summer insolation in mid- to high northern latitudes due to orbital cycles, and it is thus naturally explained by the Milankovitch theory of glaciations. Between the LGM and the beginning of the Holocene ~10 kyears BP, peak northern summer insolation increased by some 40–50 W/m^2. This massive increase in solar heating was the driver of Northern Hemisphere deglaciation and consequent sea-level rise by

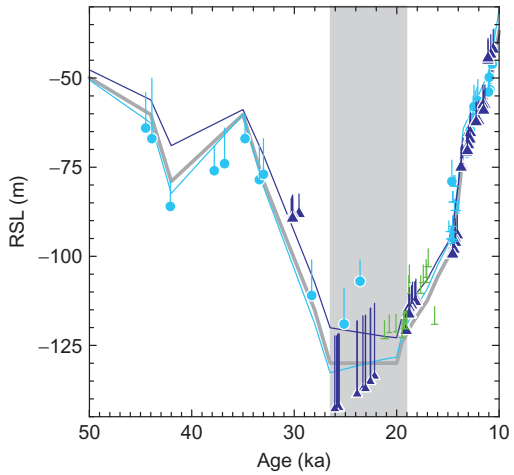

FIGURE 2.7 Sea-level reconstructions from four different sites (dots with depth uncertainty bars): New Guinea (blue dots), Sunda Shelf (blue half-pluses), Barbados (purple), Bonaparte Gulf (green). The blue and purple lines show sea-level predictions for New Guinea and Barbados, while the gray line shows eustatic sea level. The vertical gray bar indicates the time of the LGM. *From Clark et al. (2009).*

~130 m. Detailed analysis reveals some episodes of exceptionally rapid sea-level rise, known as meltwater pulses (Fairbanks, 1989). The most prominent is meltwater pulse 1A at 14.5 kyears BP, with an estimated sea-level rise of about 20 m at a rate reaching 4 m per century (Stanford et al., 2006; Deschamps et al., 2012). Clark et al. (2009) argue that meltwater pulse 1A included a major meltwater contribution from the West Antarctic Ice Sheet.

A comparison of glacial sea-level proxies with $\delta^{18}O$ from benthic foraminifera shells (the often-used Lisiecki–Raymo stack (Lisiecki and Raymo, 2005)) reveals some differences that can be explained by changes in deepwater temperature, since the calcite $\delta^{18}O$ depends on both ice volume and local temperature (Section 2.1.2). This difference suggests that deep ocean temperatures during the LGM must have been ~3 °C colder than today, and hence close to the freezing point of seawater.

Because of the relatively good availability of data, the large climate change signal, and relatively stable climate conditions over several millennia, the LGM was the target of the earliest proxy reconstructions of paleo-ocean circulation (Duplessy et al., 1988) and of a number of time slice climate model experiments with atmosphere models, with ocean models and with coupled ocean–atmosphere models, including systematic model intercomparison studies (Braconnot et al., 2007a,b). Figure 2.8 (left) shows the distribution of $\delta^{13}C$ in the modern and LGM Atlantic ocean, as a nutrient-like tracer of water masses (see Section 2.1.1). The $\delta^{13}C$ distribution of the modern ocean reflects the spread of the well-known water masses NADW and AABW. The LGM Atlantic likewise shows a low-nutrient water mass of northern origin and below it a high-nutrient water mass, but their boundary is higher up in the water column at about 2 km depth. The northern water mass is sometimes called glacial North Atlantic intermediate water (GNAIW); it can be interpreted as a shoaling of the flow of NADW which leaves room for a northward and upward extension of AABW during the LGM. This distribution of water masses was more recently confirmed by Cd/Ca ratios (Lynch-Stieglitz et al., 2007). More recent and detailed compilations of LGM proxy data also show a presence of AAIW in the Atlantic, the northward extent of which is subject to ongoing research. $\delta^{18}O$ data at 30 °S from the eastern and western side of the basin indicate a collapse of the east–west density gradient, which currently characterizes the outflow of NADW (see Section 2.1.3). While the protactinium/thorium ratio suggests a NADW renewal rate similar to today, these $\delta^{18}O$ data may indicate a much reduced NADW outflow into the Southern Ocean (Lynch-Stieglitz et al., 2007). Reconstructions of surface properties of the northern Atlantic at the same time suggest that NADW (or GNAIW) formation probably occurred to the south of the Greenland–Iceland–Scotland ridge during the LGM (Oppo and Lehman, 1993; Alley and Clark,

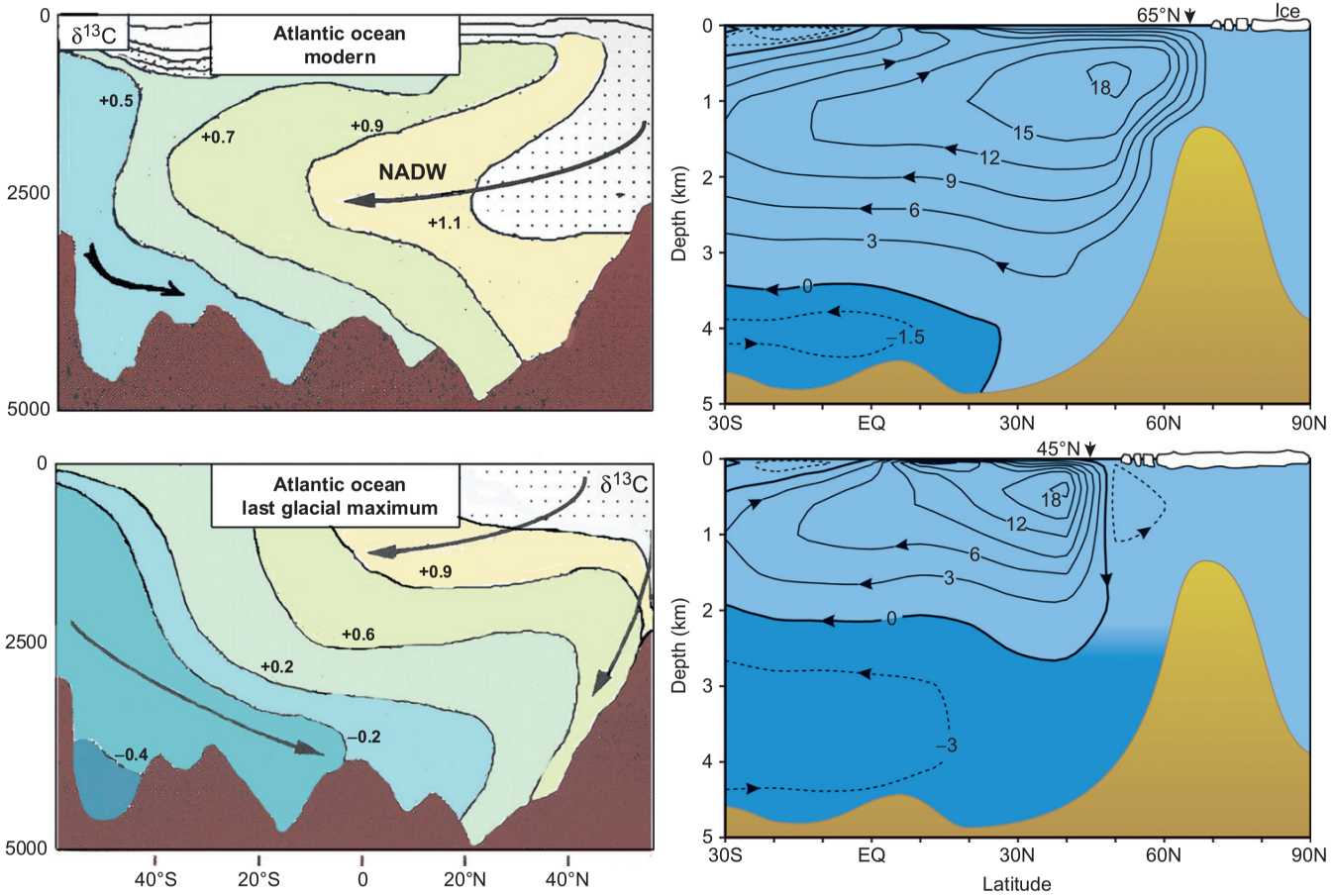

FIGURE 2.8 Left: Distribution of $\delta^{13}C$ in the modern and LGM Atlantic Ocean from Duplessy et al. (1988). Right: Stream function of Atlantic Ocean circulation for modern and LGM conditions in the climate model of Ganopolski et al. (1998). Dark blue shading indicates bottom water of Antarctic origin, brown the bottom topography.

1999), consistent with a southward extension of sea ice cover and in contrast to the modern ocean where it partly forms in the Nordic Seas and then overflows this ridge.

The first coupled ocean–atmosphere model simulation of LGM climate (Ganopolski et al., 1998), at the time still with prescribed continental ice sheets, produced an LGM circulation in the Atlantic broadly consistent with these proxy findings (see Figure 2.8). We can see a southward shift of deepwater formation, a shoaling of NADW flow and an upward and northward extension of AABW, and a similar NADW renewal rate as at present, combined with a near-breakdown of the outflow across 30 °S as the overturning cell recirculates within the Atlantic. This flow pattern is consistent with recent findings of a reversed gradient in the $^{231}Pa/^{230}Th$ ratio between north and south Atlantic during the LGM (Negre et al., 2010).

However, subsequent attempts at modeling LGM climate, including those for the Paleoclimate Modeling Intercomparison Project, have produced a variety of circulation patterns for the LGM Atlantic (Weber et al., 2007). This is perhaps not surprising since the stability properties of the thermohaline ocean circulation are highly nonlinear and dependent on a subtle density balance, where particularly the freshwater budget is difficult to get right in models even for the modern ocean (Hofmann and Rahmstorf, 2009). Systematic comparison of model results with the full suite of proxy data is needed to establish what range of circulation patterns is consistent with the data.

3.2. Abrupt Glacial Climate Changes

While the LGM was a period of frosty climate stability lasting for several 1000 years, the glacial time before the LGM as well as the period of deglaciation following the LGM were rather turbulent, punctuated by abrupt and massive, large-scale climate changes. An illustration is given in Figure 2.9, based on Greenland ice core data (often shown as standard because of their high resolution) and sediment data from the subtropical North Atlantic. The numbered warm events there are known as Dansgaard–Oeschger (DO) events while H1...H6 refers to Heinrich events, defined as episodes of massive continental ice discharge into the northern Atlantic as documented by ice-rafted debris in sediment cores. They could either result from internally or externally triggered ice sheet instability. Heinrich events do not stand out in Greenland temperature but tend to occur during cold periods preceding some strong DO events.

There is plentiful and strong evidence linking these abrupt climate events to changes in Atlantic Ocean circulation, reviewed, for example, in Alley (2007). From a mechanistic point of view, the perhaps most compelling piece of evidence for a major role of ocean heat transport changes is the "bipolar seesaw" (or "seasaw"): an antiphase behavior between the North Atlantic and the Southern Ocean/Antarctica (Stocker, 1998). Establishing the phase relationship required accurate relative dating between distant paleoclimatic records, which was achieved for Greenland and Antarctic ice cores using the globally synchronous variations in atmospheric methane that are recorded at both poles (Blunier and Brook, 2001; Figure 2.10). Methane changes must be synchronous since methane is a well-mixed greenhouse gas in the atmosphere, so they can be used to line up the records. Examination of the phase relation shows that during cold phases in Greenland (termed "stadials") Antarctic temperature increases, while at the time of abrupt warming in Greenland (the DO events) Antarctic temperature begins to drop and then continues to decline during Greenland warm phases (called interstadials).

The same pattern is found in climate model simulations in response to changes in the Atlantic meridional overturning circulation (Ganopolski and Rahmstorf, 2001; see Figure 2.11). This behavior can be nicely explained by a simple conceptual model consisting of changes in northward ocean heat transport coupled to a heat reservoir in the south, the Southern Ocean (Stocker and Johnsen, 2003).

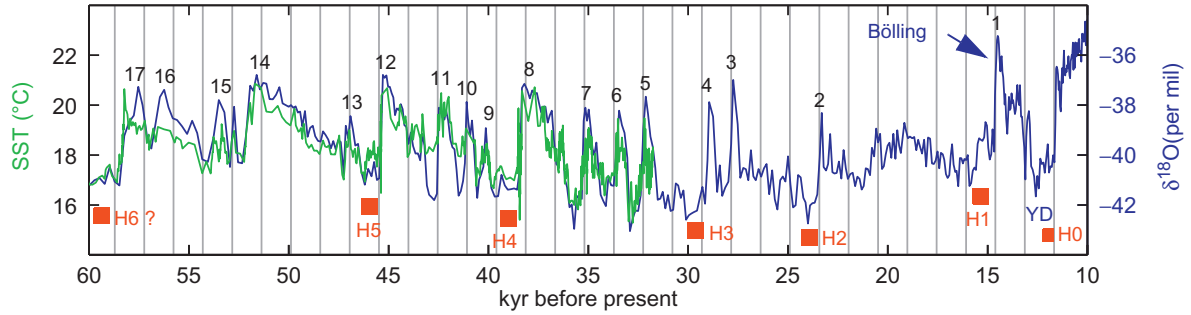

FIGURE 2.9 Proxy data from the subtropical Atlantic (green) (Sachs and Lehman, 1999) and from the Greenland ice core GISP2 (blue) (Grootes et al., 1993) show several Dansgaard–Oeschger (D/O) warm events (numbered). The timing of Heinrich events is marked in red. Gray lines at intervals of 1470 years illustrate the tendency of D/O events to occur with this spacing, or multiples thereof.

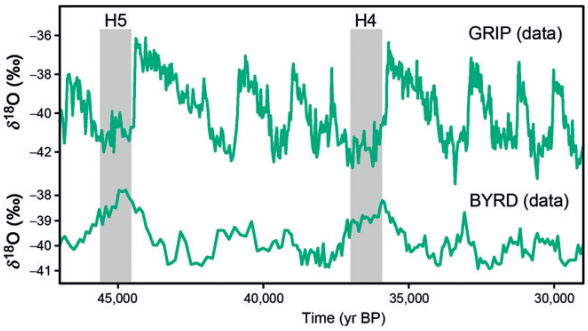

FIGURE 2.10 Oxygen isotopes as a temperature proxy for the Greenland ice core of GRIP and the Byrd ice core in Antarctica, synchronized on a common time scale. Graph by A. Ganopolski after (Blunier and Brook, 2001). Heinrich events 4 and 5 are marked as in Figure 2.9.

Subsequent more detailed data, including also millennial events from the previous glacial period, support this concept, showing a magnitude of Antarctic response that asymptotically approaches an equilibrium with increasing duration of North Atlantic stadials (Margari et al., 2010).

While compelling evidence thus points to ocean heat transport changes at the core of abrupt glacial climate events, the exact nature of these ocean circulation changes is harder to establish. The simple concept of a bistable AMOC, which is either turned "on" or "off," clearly does not have enough degrees of freedom to explain glacial and modern circulations as well as DO and H events. Neither does the concept of an AMOC that simply has different flow rates appear to explain the data. For example, why are DO warmings in Greenland so abrupt? Why do Heinrich events appear as prominent cooling at the Portuguese margin (Cacho et al., 1999) but not in Greenland (Figure 2.9)? And why are DO events associated with a large salinity increase near Iceland (Kreveld et al., 2000)?

One possible explanation for these features is a concept with three distinct circulation modes and transitions between them (see schematic Figure 2.12), which is based on time slice reconstructions using sediment cores (Sarnthein et al., 1994) as well as model experiments (Ganopolski and Rahmstorf, 2001). The central image shows a "cold mode" of the AMOC prevailing during the LGM and stadial periods. DO events occur when convection starts in the Nordic Seas (a situation that is stable in the Holocene but only metastable during glacial conditions, that is, in the latter case the circulation reverts spontaneously to the cold mode after some hundreds of years), which extends the AMOC northward, reduces sea ice cover there, and leads to strong warming over Greenland. This mechanism can explain the salinity increase during DO events (Figure 2.11b) and the shape and phasing of Greenland and Antarctic temperatures (Figure 2.11d and e). DO events can thus be viewed as a "flickering" between the Holocene and LGM modes of the AMOC, where the latter is the stable one during glacial

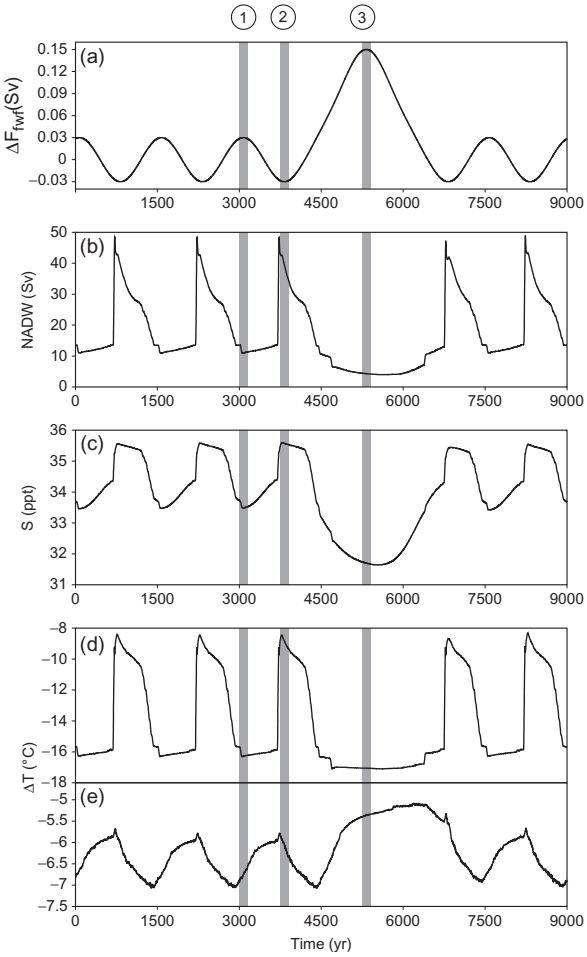

FIGURE 2.11 Simulated DO and Heinrich events. (a) Forcing, (b) Atlantic overturning, (c) Atlantic salinity at 60 °N, (d) air temperature in the northern North Atlantic sector (60–70 °N), and (e) temperature over Antarctica (temperature values are given as the difference from the present-day climate, ΔT). *From Ganopolski and Rahmstorf (2001).*

times. Other modeling attempts have been reviewed by Kageyama et al. (2010).

Heinrich events can be interpreted as a temporary shutdown of North Atlantic deepwater formation and flow, caused by a dilution of northern Atlantic surface waters due to meltwater release stemming from the iceberg discharge events (Otto-Bliesner and Brady, 2010). Such a shutdown would lead to cooling of the North Atlantic (but perhaps hardly affecting Greenland, since ocean heat transport already does not reach that far north in the cold mode) and warming in Antarctica, asymptotically approaching an equilibrium as seen in Figure 2.11e and in ice core data (Margari et al., 2010).

An interesting discussion has arisen about the timing of DO events, many of which tend to occur in intervals

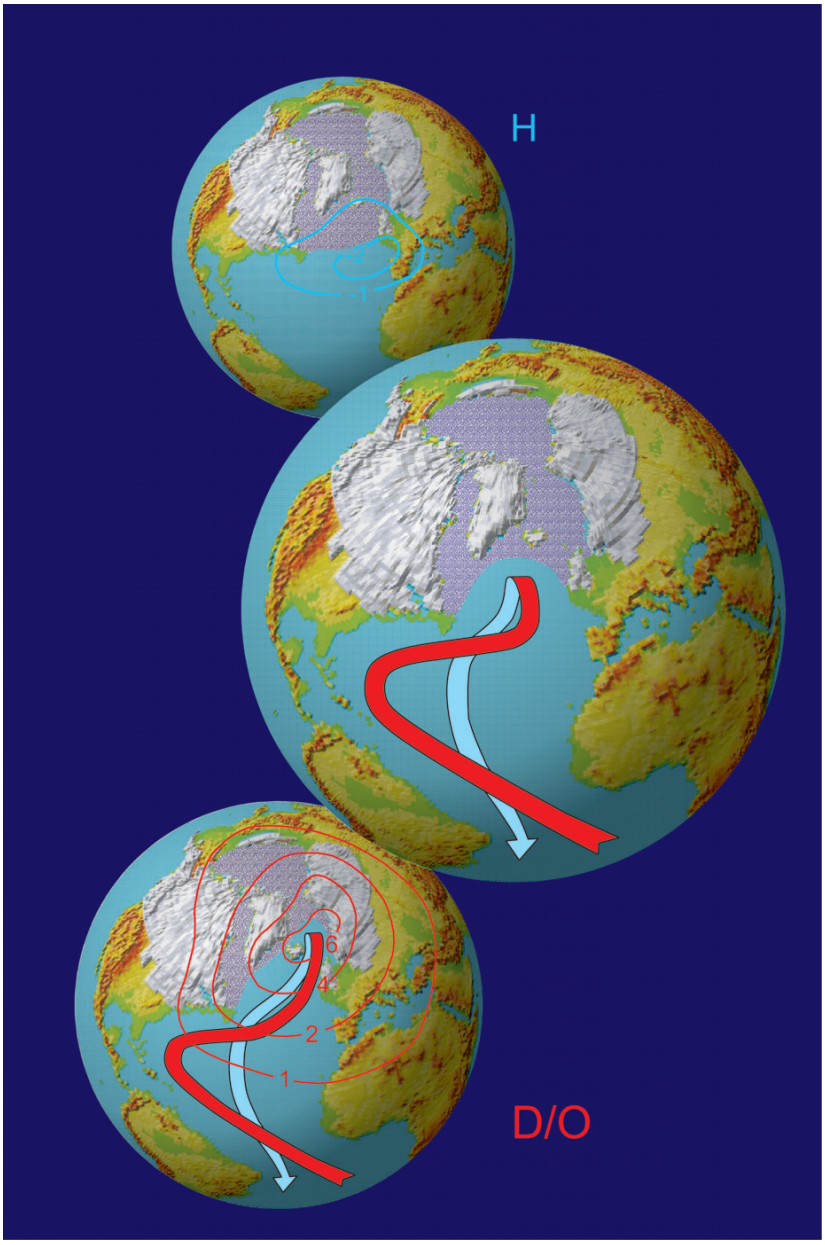

FIGURE 2.12 Schematic of the three circulation modes explained in the text.

of 1500 years or multiples thereof (see the gray lines in Figure 2.9; Alley et al., 2001a; Schulz, 2002; Rahmstorf, 2003). A physical mechanism that can produce such a timing is stochastic resonance (Gammaitoni et al., 1998; Alley et al., 2001a,b; Ganopolski and Rahmstorf, 2002). Model simulations suggest that solar cycles could provide the weak regular trigger required by the stochastic resonance mechanism (Braun et al., 2005).

3.2.1. *Deglaciation*

Since the late 1990s and based on an increasingly large number of proxy records, the time history of deglaciation (the transition from the last ice age into the Holocene) has been interpreted as a globally near synchronous warming out of the ice age (synchronized in part by the global atmospheric CO_2 increase), superimposed with a

north–south seesaw due to episodic changes in the Atlantic overturning circulation (Alley and Clark, 1999; Clark et al., 2002; Rahmstorf, 2002). During deglaciation, the melting of the ice sheets may have provided an irregular freshwater input disrupting the Atlantic Ocean circulation. The most recent data compilations have firmed up that interpretation and added much detail (Barker et al., 2009; Clark et al., 2012). In line with early model results for the response of the AMOC to freshwater forcing, they document an immediate antiphase response off South Africa and more gradual changes in Antarctica. Thus, a major role of AMOC changes in shaping the climate evolution during deglaciation can now be considered well established, thanks to the consistent picture that has emerged from many high-resolution proxy records as well as model simulations. Details of the sequence of events are still subject to active research.

3.3. Glacial Cycles

The prime characteristic of glacial cycles is the growth and decay of vast continental ice sheets, directly mirrored in the global ocean in the form of sea-level and salinity changes. Since the average depth of today's global ocean is 3790 m, the 130-m sea-level drop during the LGM amounts to ~3.5% of all ocean water being removed and stored on land, increasing the average salinity of the remaining ocean water by over 1 psu and increasing its average $\delta^{18}O$ content by 1.0‰ ± 0.1‰ (Clark et al., 2009).

Figure 2.13 shows a reconstruction of eustatic sea-level changes over the last four glacial cycles based mainly on $\delta^{18}O$ and coral data. To first order, it shows a sawtooth pattern with a slow descent into full glacial conditions but comparatively rapid deglaciations, which can be explained by a fundamental asymmetry in ice sheet physics: continental ice sheets grow slowly by accumulating snow at their surface, but they can decay much more rapidly due to a combination of surface melting and ice flow (i.e., solid ice discharge into the ocean).

Figure 2.14 shows a recent attempt at modeling the last glacial cycle with an intermediate complexity coupled climate model driven by variations of the Earth's orbital parameters and atmospheric concentration of major greenhouse gases prescribed from ice core data (Ganopolski et al., 2010). The model contains a three-dimensional polythermal ice sheet model which successfully reproduces the history of ice sheet growth and decay and hence sea level, as shown in the figure, with some underestimation of the maximum ice sheet volume. The oscillations superimposed on the basic sawtooth shape result from the precession cycle in the orbital parameters which has a period of 23 kyears.

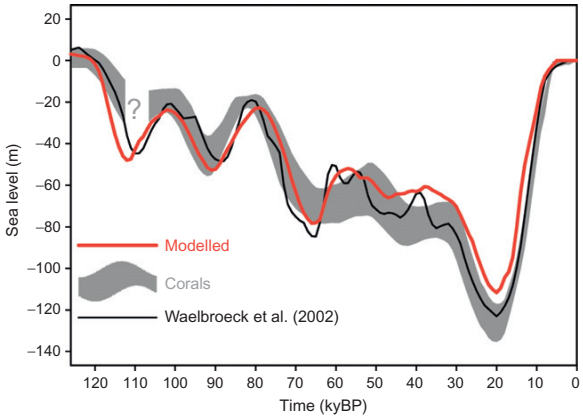

FIGURE 2.14 Simulation of the last glacial cycle with the CLIMBER-2 ocean–atmosphere ice sheet model compared to the data shown in Figure 2.13. *From Ganopolski et al. (2010).*

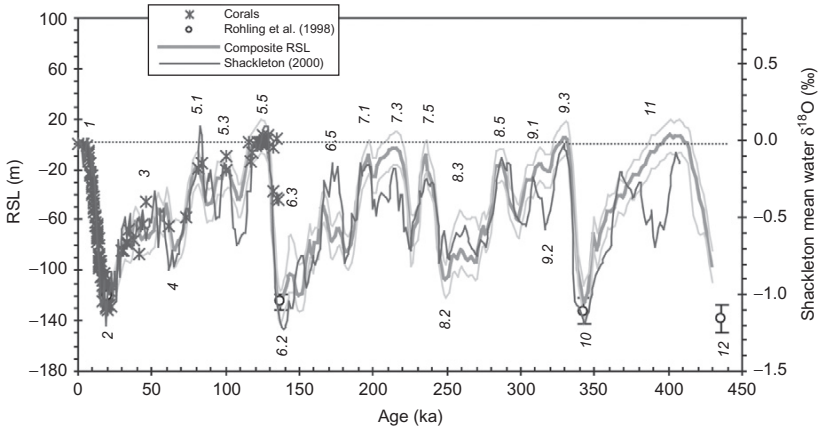

FIGURE 2.13 Left axis: Composite RSL curve (bold gray line) and associated confidence interval (thin gray lines). Crosses: coral reef relative sea-level data. Empty circles: Relative sea-level low stands estimated by Rohling et al. (1998). Right axis: variations in mean ocean water $\delta^{18}O$ derived by Shackleton (2000) from atmospheric $\delta^{18}O$ (black line). *Graph from Waelbroeck et al. (2002).*

A remaining challenge is to produce such simulations with predicted rather than prescribed greenhouse gas concentrations.

In the course of glacial cycles, ocean circulation changes have mainly been discussed with respect to abrupt events within the glacial and the specific sequence of events during the last deglaciation (see Section 3.2.1). However, if a weakening of the Atlantic overturning circulation is a general feature of the transitions from glacial to interglacial conditions, due to the massive northern meltwater input occurring at these times, then the bipolar seesaw may be part of the explanation of the time lag of atmospheric carbon dioxide concentration behind Antarctic temperature that is found in Antarctic ice cores (Ganopolski and Roche, 2009).

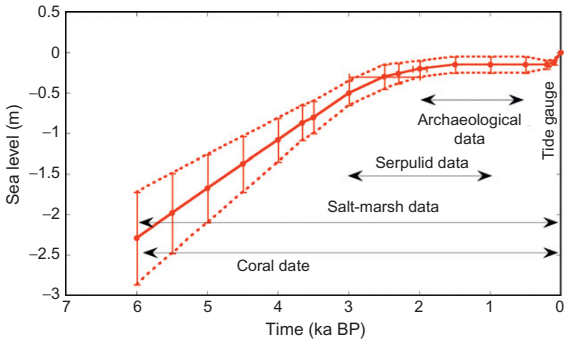

FIGURE 2.15 Current best estimates, including uncertainty estimates, of the eustatic sea-level change over the past 6000 years, as inferred from geological and archaeological data and from the tide gauge data for the past century. *From Lambeck et al. (2010).*

3.4. Interglacial Climates

Conditions during the current Holocene and previous interglacials do not differ as dramatically from modern climate as do glacial conditions, so it is more difficult to establish what changes in ocean circulation—if any—may have occurred. Global mean temperature likely was no more than 1.5 °C warmer than in the preindustrial time, if at all, although regional differences were larger (Turney and Jones, 2010; McKay et al., 2012). Lynch-Stieglitz et al. (2009) have attempted to reconstruct the flow of the Florida current over the past 8000 years from oxygen isotope data and found a small increase of 4 Sv (out of a total of ~30 Sv) over this period. Given this small change and the uncertainties of the proxy method, the main (and also interesting) conclusion probably is that the flow was rather stable over the last 8000 years.

Most discussion on interglacial climates has focused on sea-level changes, both over the Holocene and in previous interglacials. Global sea level during the Eemian interglacial, ~120,000 years BP, has been estimated as peaking at 5.5–9 m above present sea level (Kopp et al., 2009; Dutton and Lambeck, 2012). This is of considerable interest in the context of current global warming since it may provide clues about the response of ice sheets to warmer climate conditions. Data from the Eemian in combination with an ice sheet model ensemble have been used to constrain the stability threshold of the Greenland ice sheet (Robinson et al., 2011). This threshold could be crossed between 0.8 and 3.2 °C global warming above preindustrial conditions, with a best estimate of 1.6 °C (Robinson et al., 2012). Discussion on Eemian sea level continues, for example, about sea-level changes within the Eemian period and about the relative contributions of the Greenland and Antarctic ice sheets (Dahl-Jensen et al., 2013).

In the Holocene, sea level is characterized by the long tail of deglaciation due to the long time scale needed for melting continental ice. Different locations record different times when the relative postglacial sea-level rise ended, due to the interplay between eustatic sea-level rise and postglacial uplift (or in some places, subsidence). Lambeck et al. (2010) have constructed a eustatic sea-level curve for the past 6000 years, based on a multitude of relative sea-level data (Figure 2.15). Their best estimate shows how postglacial sea level rise came to an end between 2 and 3 kyears BP, after which sea level was approximately constant until the modern rise, registered by the tide gauges, started.

A compilation of relative sea-level records for the last two millennia from different parts of the world is shown in Figure 2.16. This shows some consistency but also large local deviations (e.g., records for Israel, Cook Islands). It is tempting to consider the consistent records as representative of eustatic sea level (the data have already been adjusted for GIA) while the deviating records are affected by local issues. More records need to be collected from different shores to build up a clearer picture.

Figure 2.17 shows proxy records from the US east coast (also shown in Figure 2.16) with an attempt to model the sea-level evolution with a semiempirical model as a function of global temperature. A successful fit is obtained for the last millennium but not the time before 1000 AD. Ongoing work suggests this may be due to the global temperature reconstruction that was used, which is warmer than others before 1000 AD and thus leads to sea-level rise in the model at a time when stable sea level is found in the proxy data.

4. THE DEEPER PAST

4.1. Challenges of Deep-Time Paleoceanography

Reconstructing the ocean circulation in the geological past becomes increasingly more difficult at earlier times. This is mainly due to the effects of plate tectonics which continuously

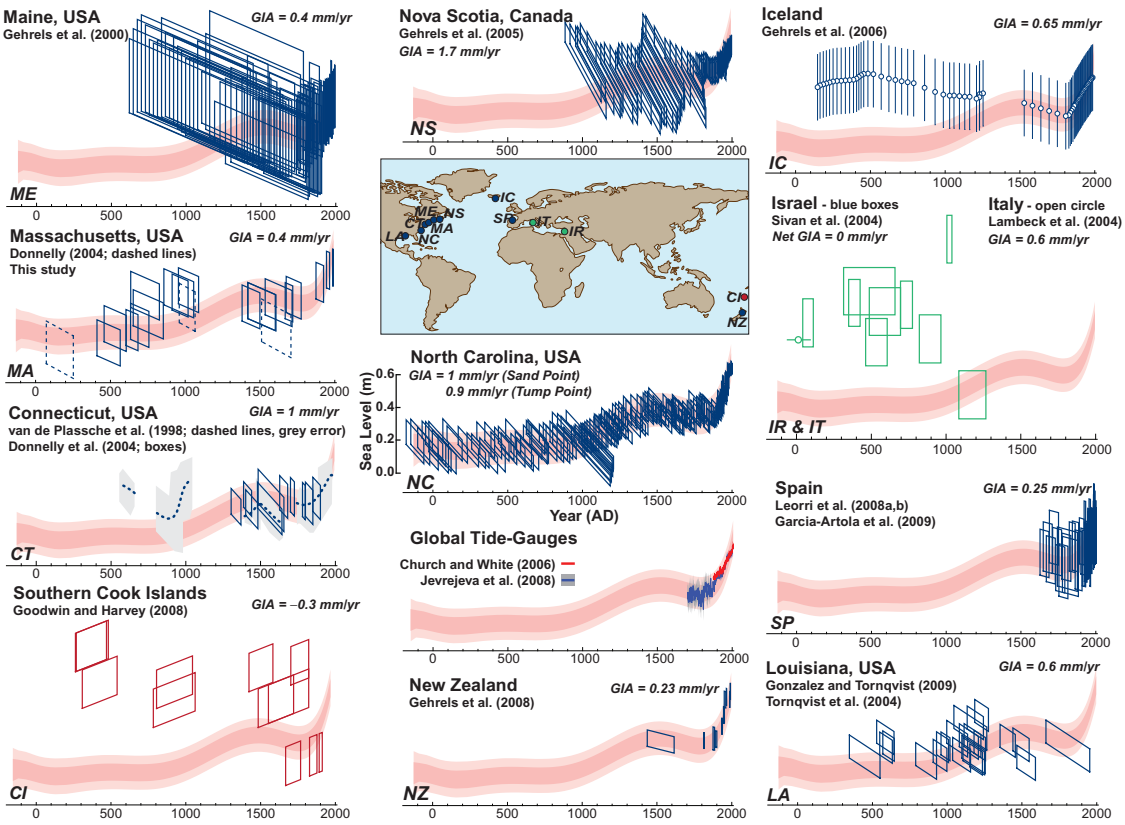

FIGURE 2.16 Late Holocene sea-level reconstructions after correction for GIA. Rate applied (listed) was taken from the original publication when possible. In Israel, land and ocean basin subsidence had a net effect of zero. Reconstructions from salt marshes are shown in blue, archaeological data in green, and coral microatolls in red. Tide gauge data expressed relative to AD 1950–2000 average. Vertical and horizontal scales for all datasets are the same and are shown for North Carolina. Datasets were vertically aligned for comparison with the summarized North Carolina reconstruction (pink). *From Kemp et al. (2011).*

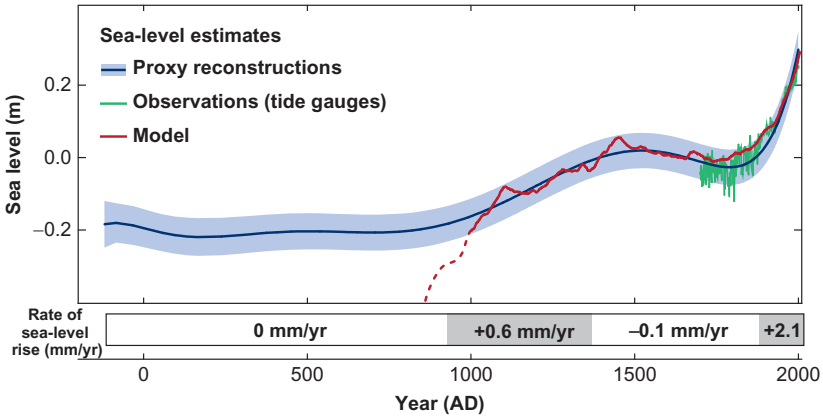

FIGURE 2.17 Sea-level reconstruction for North Carolina from salt marsh data (as in Figure 2.16, here shown blue) compared to tide gauge data (green) (Jevrejeva et al., 2006) and a semiempirical model (red). *From Kemp et al. (2011).*

change the position of continents and the topography of the ocean floor on geological timescales, both of which have a direct influence on ocean circulation. In contrast to the oceans in the Quaternary (Section 3), accurate paleogeographic reconstructions are therefore a prerequisite for understanding the ocean circulation during Earth's deeper past.

For the past 150 million years or so, paleogeographic reconstructions mostly rely on magnetic anomalies imprinted into the ocean floor and on the positions of the relatively stable mantle plumes. Unfortunately, these proxies are not available for earlier times, because oceanic crust is continuously formed at mid-ocean ridges and later returned to the mantle at subduction zones. In fact, the oldest parts of the ocean floor date back to the Jurassic period (200–146 million years ago), with the majority being much younger (Müller et al., 2008a; see Figure 2.18). For earlier times, paleogeographic reconstructions have to rely on paleomagnetic data (indicating the latitude and orientation of continents) and paleontological records (indicating the geographic distribution of species), making paleogeographic maps increasingly uncertain beyond the Cretaceous (146–66 million years ago) (Cocks and Torsvik, 2002; Torsvik and Cocks, 2004).

The continuous recycling of the oceanic crust also limits the sedimentary record and thus the availability of tracers of past ocean circulation (see Section 2.2), again making the Cretaceous the earliest time for which the physical state of the ocean can be investigated in detail. As a matter of fact, the Cretaceous with its warm greenhouse climate and small meridional temperature gradient is also a particularly interesting period in Earth's history. In particular, it has been suggested that the ocean circulation in the Cretaceous could have been radically different from today. The remainder of this section therefore concentrates on the climate during the Cretaceous and briefly reviews research on the ocean circulation during this time.

4.2. The Oceans During the Mid-Cretaceous Warm Period

Temperature reconstructions indicate that the global average surface air temperature was above modern levels for the entire Cretaceous, with particularly strong warming around 95 million years ago, when global surface air temperatures were about 20 °C warmer than today (Figure 2.19). In the following, we focus on ocean circulation during this mid-Cretaceous warm period, beginning with a look at the continental configuration at that time.

A reconstruction for the paleogeography during the mid-Cretaceous (90 million years ago) is shown in Figure 2.20. At that time, the break-up of the supercontinent Pangaea, which had begun in the Jurassic, has progressed to a point where continental landmasses known today had separated from each other, although in many cases only separated by narrow and very shallow seas. Note that the distribution of continents and the absence or presence of open ocean gateways can be of considerable importance for Earth's climate. The opening of the passages around Antarctica, for example, likely played a major role in the growth of its ice sheet and thus for the global and regional energy balance (Kennett, 1977).

One particularly striking feature of the geography during that period are epicontinental (or epeiric) seas, shallow seas covering large parts of what would later become continental North America, Europe, and Africa. This Cretaceous transgression is thought to be primarily caused by rapid seafloor spreading at mid-ocean ridges, which reduced the volume of ocean basins and thus led to a rise in eustatic sea level (Hays and Pitman, 1973). Estimates of mid-Cretaceous sea levels differ widely, however, roughly covering a range from 50 to 250 m above present day (Miller et al., 2005; Müller et al., 2008b).

Early model simulations indicated that the changes in paleogeography (as compared to present day) alone can account for about 5 °C warming during the mid-Cretaceous (Barron and Washington, 1984). Later studies, however, found only a minor contribution to the observed warming (Barron et al., 1995; Bice et al., 2000). Higher levels of atmospheric greenhouse gases (in particular carbon dioxide) are thought to explain the bulk of the warming during the Cretaceous.

Mid-Cretaceous atmospheric carbon dioxide levels can be estimated from proxy data and models of the global carbon cycle. Empirical estimates rely on $\delta^{13}C$ carbon isotope ratios in paleosols, alkenones, or planktonic foraminifera, distribution of stomatal pores in C3 plants, or $\delta^{11}B$ boron isotope ratios in planktonic foraminifera (Royer, 2006). As shown in Figure 2.21, atmospheric carbon dioxide concentrations during the middle Cretaceous were around 1000 ppm and thus significantly higher than today, albeit with a large uncertainty range (roughly 500–1500 ppm). A strong contribution of the higher carbon dioxide levels (possibly enhanced by methane) to the observed warming is therefore very likely. The geological record also indicates an ice-free world during the Jurassic and Cretaceous. These time periods are therefore an ideal testbed to study the internal dynamics of a climate system without polar icecaps.

Concerning geographic patterns, temperature proxy data for the mid-Cretaceous indicate tropical temperatures a few degrees warmer than today (possibly up to 40 °C), but significantly warmer polar regions. As for other warm periods in Earth's history, the mid-Cretaceous is therefore characterized by a significantly reduced meridional temperature gradient often referred to as an "equable" climate (Crowley and Zachos, 2000; Hay, 2008). For illustration, Figure 2.22 shows an example of a proxy-based latitudinal temperature distribution during the late Cretaceous as

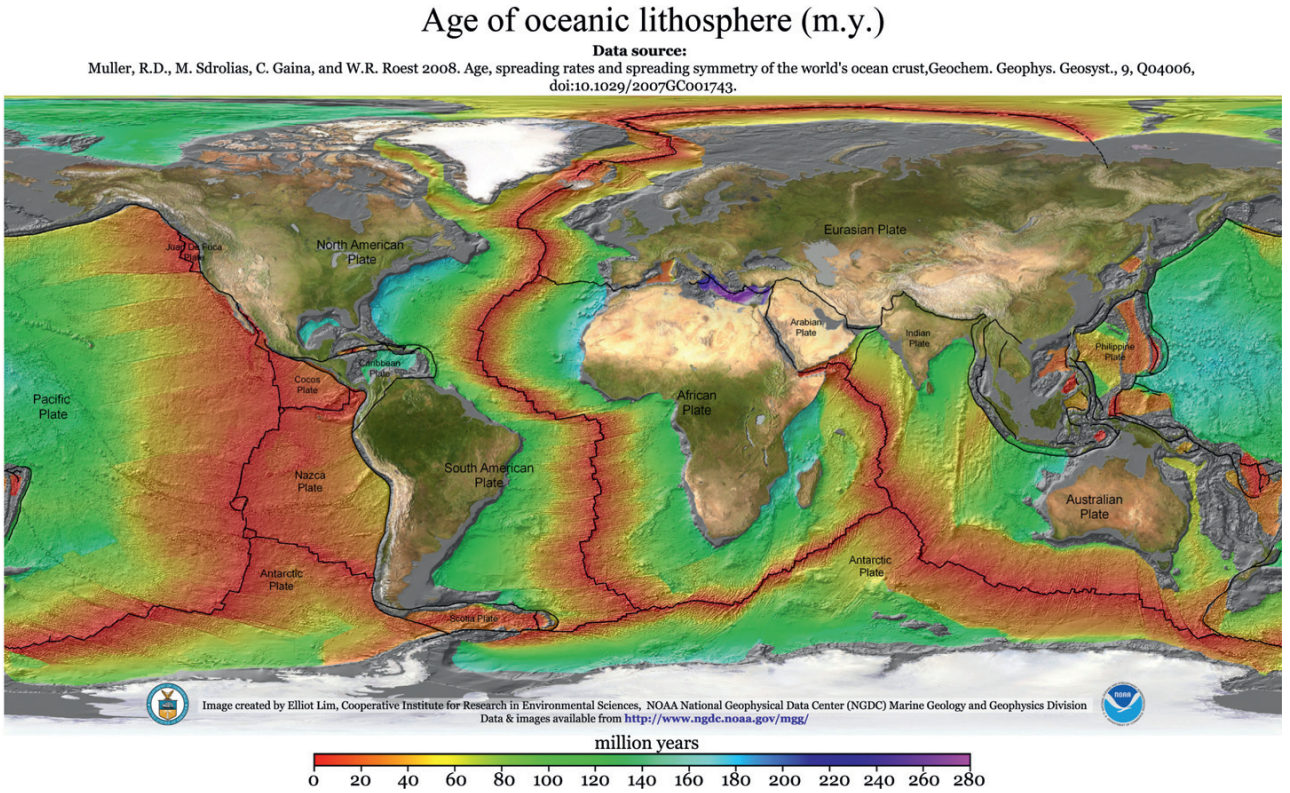

FIGURE 2.18 Age distribution of the oceanic crust on Earth. *Source: NOAA.*

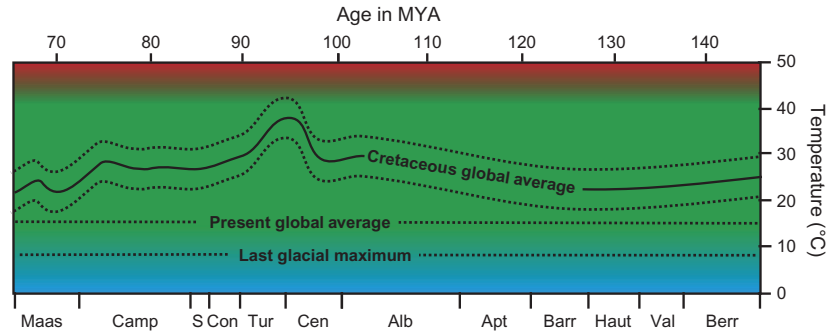

FIGURE 2.19 Schematic view of reconstructed global surface air temperatures during the Cretaceous. *Reproduced from Hay and Floegel (2012).*

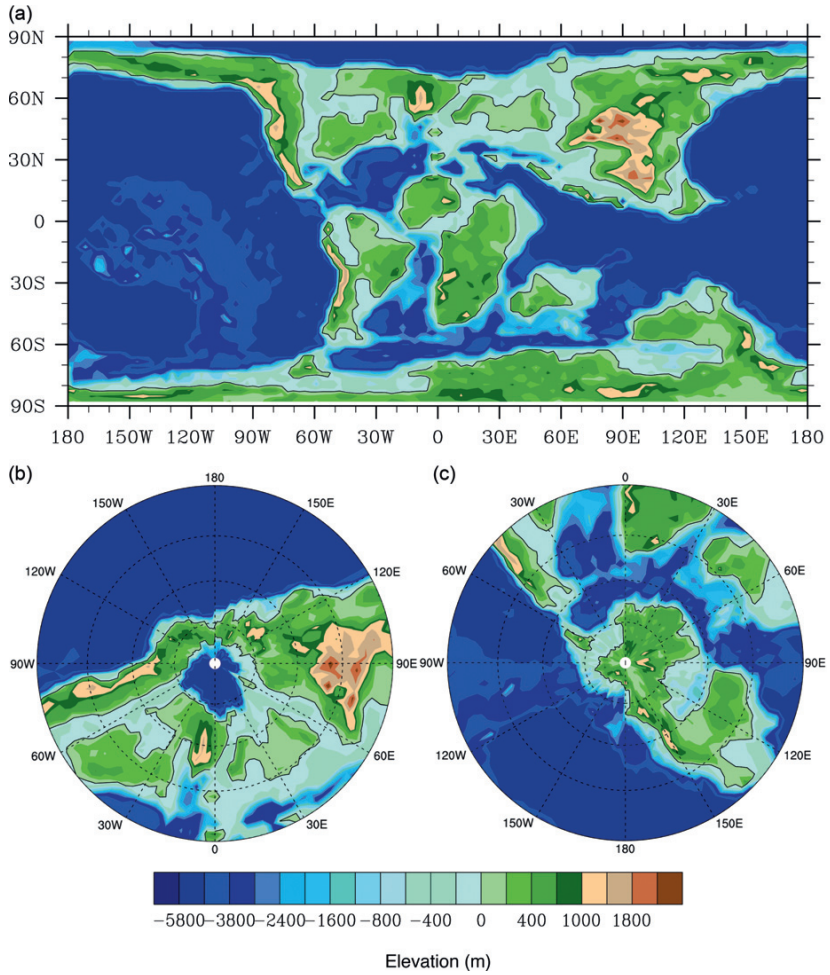

FIGURE 2.20 Paleogeography (elevation in meters) during the mid-Cretaceous (90 million years ago) in cylindrical (a), North polar (b), and South polar (c) projections (Sewall et al., 2007).

compared to the present-day climate. (Note that earlier studies had indicated an even flatter Cretaceous temperature gradient with "cool tropics," but this interpretation has now been shown to be biased by diagenesis, see, e.g., Pearson et al., 2001).

Equable climates during previous warm periods (and in particular during the Cretaceous) have received considerable attention because climate model experiments have generally had difficulties in reproducing the latitudinal temperature distribution inferred from proxy data

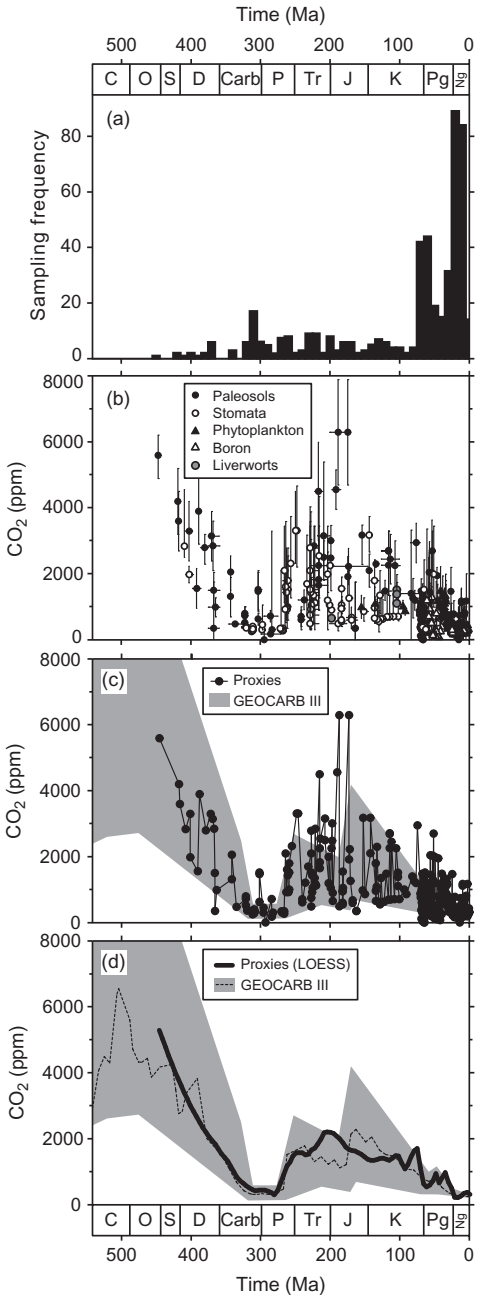

FIGURE 2.21 Sampling frequency (panel a) for proxy data for the evolution of atmospheric carbon dioxide concentrations during the Phanerozoic (the past 542 million years) as shown in panel b. Panel c: comparison of the proxy data (black) with results from carbon cycle modeling (gray, with uncertainty range). Panel d: comparison of best-guess prediction of the carbon cycle model (dashed line, range indicated by gray shading) with the smoothed proxy record (black). *Reproduced from Royer (2006).*

(Crowley and Zachos, 2000). It has often been suggested that an increased meridional heat transport in the ocean could have caused the reduced temperature gradient in the Cretaceous. One hypothesis postulates that—in contrast to the present-day situation —deepwater formation could have taken place at low latitudes, with warm saline water masses transported at depths toward the poles (Chamberlin, 1906). Model simulations for the Cretaceous do not support this hypothesis, however, and yield conflicting results concerning the open ocean sites of deepwater formation. Emanuel (2001) suggests that the higher intensity of tropical cyclones following an increase in tropical temperatures could lead to stronger vertical mixing in the tropics, resulting in an increased ocean heat transport toward the poles. Hotinski and Toggweiler (2003) propose that the presence of a circumglobal ocean passage at low latitudes could increase the meridional heat transport in the Cretaceous oceans. This hypothesis is another example of the more general importance of ocean gateways for ocean circulation and climate. Hays (2008) argues that a significant contribution from many sources of deepwater along the margins of the wide-spread shallow seas in the Cretaceous may be expected. This lack of a truly global overturning circulation could also help explain the evidence for ocean anoxia observed in the sedimentary record as frequent occurrences of black shales (Hay, 2008).

Clearly, much remains to be done to better understand the role of the ocean circulation for the equable climate problem. However, other factors could have contributed to the shallow temperature gradient. Forest expansion during in the Cretaceous has been shown to lead to high-latitude warming, for example (Otto-Bliesner and Upchurch, 1997; Zhou et al., 2012). Further, an increased meridional transport of latent heat in the atmosphere or changes in the radiative balance of mid and high latitudes have been suggested to contribute to the equable climate during the Cretaceous. For example, Abbot et al. (2009) suggest a high-latitude positive cloud feedback mechanism in which high-latitude warming leads to increased atmospheric convection, resulting in decreased cooling (or even warming) by clouds at high latitudes and thus a more equable climate. Further, coupled oceanic–atmospheric processes could be important. Rose and Ferreira (2013) propose that enhanced ocean heat transport could drive strong atmospheric convection in the mid-latitudes, leading to warming up to the poles due to higher humidity in the upper troposphere.

More detailed simulations with coupled Earth system models could shed further light on the processes responsible for the equable climate problem and on the role of the oceans in the Cretaceous climate system.

5. OUTLOOK

The proxy data and model results discussed here give an impression of the formidable detective work that is required to find and decipher information about past ocean states. Both proxy data and models are difficult and time-consuming to develop and understand, and their results are not always easy to interpret. Mistakes and blind alleys

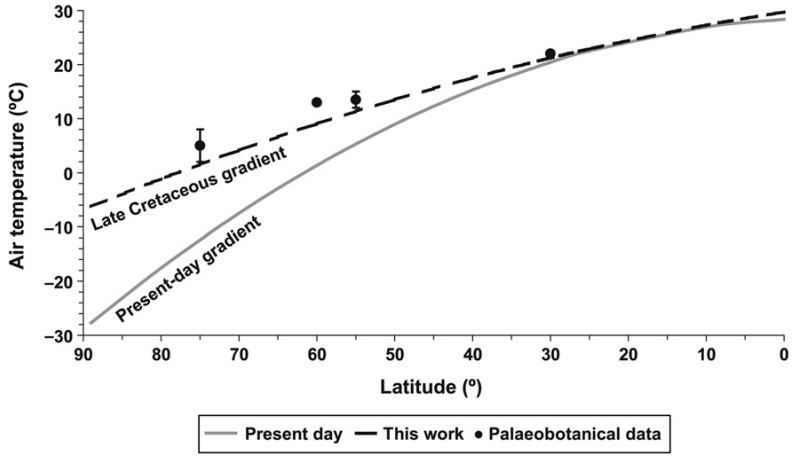

FIGURE 2.22 Example of a shallow temperature gradient during the late Cretaceous: temperature as a function of absolute paleolatitude based on $\delta^{18}O$ of fossil continental vertebrates (dashed line) and paleobotanical data (circles) as compared to the present-day gradient (gray line). *Reproduced from Amiot et al. (2004).*

are an inevitable part of this slow learning process. Yet, we hope we have been able to convince the readers that these efforts pay off and that slowly, more and more robust and precise information is emerging. This information about past climate and oceans is crucial for a better understanding of the rapid climate changes we are witnessing (and causing) at present.

The effort on paleoclimatic research is thus an effort well spent. While there are still more questions than answers, there is great promise that further painstaking work will be able to clarify many of the issues that still seem puzzling today. A better knowledge of the past is vital for an improved understanding of the dynamics of the Earth system, and it thus helps to provide the kind of knowledge humanity needs for a sustainable stewardship of our home planet.

ACKNOWLEDGMENTS

We thank Jean Lynch-Stieglitz and Kurt Lambeck for their excellent review articles, which greatly helped in the preparation of this book chapter. We also thank Andrew Kemp and Ben Horton for introducing us to sea-level proxies, and many colleagues, particularly Andrey Ganopolski, Michael Mann, Eric Steig, and Gavin Schmidt, for numerous discussions on paleoclimate.

REFERENCES

Abbot, D.S., Huber, M., Bousquet, G., Walker, C.C., 2009. High-CO2 cloud radiative forcing feedback over both land and ocean in a global climate model. Geophys. Res. Lett. 36, L05702. http://dx.doi.org/10.1029/2008GL036703.

Adkins, J.F., Cheng, H., Boyle, E.A., Druffel, E.R.M., Edwards, R.L., 1998. Deep-sea coral evidence for rapid change in ventilation of the deep North Atlantic 15,400 years ago. Science 280 (5364), 725–728. http://dx.doi.org/10.1126/science.280.5364.725.

Allen, J.R.L., 2000. Morphodynamics of Holocene salt marshes: a review sketch from the Atlantic and Southern North Sea coasts of Europe. Quat. Sci. Rev. 19 (12), 1155–1231. http://dx.doi.org/10.1016/s0277-3791(99)00034-7.

Alley, R.B., 2007. Wally was right: predictive ability of the North Atlantic "Conveyor belt" hypothesis for abrupt climate change. Annu. Rev. Earth Planet. Sci. 35, 241–272. http://dx.doi.org/10.1146/annurev.earth.35.081006.131524, Annual Review of Earth and Planetary Sciences. Annual Reviews, Palo Alto.

Alley, R.B., Clark, P.U., 1999. The deglaciation of the northern hemisphere: a global perspective. Annu. Rev. Earth Planet. Sci. 27, 149–182.

Alley, R.B., Anandakrishnan, S., Jung, P., 2001a. Stochastic resonance in the North Atlantic. Paleoceanography 16, 190–198.

Alley, R.B., Anandakrishnan, S., Jung, P., Clough, A., 2001b. Stochastic resonance in the North Atlantic: further insights. In: Seidov, D., Maslin, M., Haupt, B.J. (Eds.), The Oceans and Rapid Climate Change: Past, Present and Future, vol. 126. AGU, Washington, pp. 57–68, Geophysical Monograph.

Alley, R., et al., 2002. Abrupt Climate Change—Inevitable Surprises. National Academy Press, Washington, p. 230.

Amiot, R., Lécuyer, C., Buffetaut, E., Fluteau, F., Legendre, S., Martineau, F., 2004. Latitudinal temperature gradient during the Cretaceous upper Campanian-middle Maastrichtian: $\delta^{18}O$ record of continental vertebrates. Earth Planet. Sci. Lett. 226, 255–272. http://dx.doi.org/10.1016/j.epsl.2004.07.015.

Anderson, R.F., Bacon, M.P., Brewer, P.G., 1983. Removal of Th-230 and Pa-231 from the Open Ocean. Earth Planet. Sci. Lett. 62 (1), 7–23. http://dx.doi.org/10.1016/0012-821x(83)90067-5.

Argus, D.F., Peltier, W.R., 2010. Constraining models of postglacial rebound using space geodesy: a detailed assessment of model ICE-5G (VM2) and its relatives. Geophys. J. Int. 181 (2), 697–723. http://dx.doi.org/10.1111/j.1365-246X.2010.04562.x.

Ballarotta, M., Brodeau, L., Brandefelt, J., Lundberg, P., Döös, K., 2013. A Last Glacial Maximum world-ocean simulation at eddy-permitting

resolution—part 1: experimental design and basic evaluation. Clim. Past Discuss. 9, 297–328.

Barker, S., Diz, P., Vautravers, M.J., Pike, J., Knorr, G., Hall, I.R., Broecker, W.S., 2009. Interhemispheric Atlantic seesaw response during the last deglaciation. Nature 457 (7233), 1097–1102. http://dx.doi.org/10.1038/nature07770.

Barron, E.J., Washington, W.M., 1984. The role of geographic variables in explaining paleoclimates: results from Cretaceous climate model sensitivity studies. J. Geophys. Res. 89, 1267–1279.

Barron, E.J., Fawcett, P.J., Peterson, W.H., Pollard, D., Thompson, S.L., 1995. A "simulation" of mid-Cretaceous climate. Paleoceanography 10, 953–962.

Bice, K.L., Scotese, C.R., Seidov, D., Barron, E.J., 2000. Quantifying the role of geographic change in Cenozoic ocean heat transport using uncoupled atmosphere and ocean models. Palaeogeogr. Palaeoclimatol. Palaeoecol. 161, 295–310.

Blunier, T., Brook, E.J., 2001. Timing of millennial-scale climate change in Antarctica and Greenland during the last glacial period. Science 291, 109–112.

Boyle, E.A., 1992. Cadmium and delta-C-13 paleochemical ocean distributions during the stage-2 glacial maximum. Annu. Rev. Earth Planet. Sci. 20, 245–287. http://dx.doi.org/10.1146/annurev.earth.20.1.245.

Boyle, E.A., Sclater, F., Edmond, J.M., 1976. Marine geochemistry of cadmium. Nature 263 (5572), 42–44. http://dx.doi.org/10.1038/263042a0.

Braconnot, P., Otto-Bliesner, B., Harrison, S., Joussaume, S., Peterchmitt, J.Y., Abe-Ouchi, A., Crucifix, M., Driesschaert, E., Fichefet, T., Hewitt, C.D., Kageyama, M., Kitoh, A., Laine, A., Loutre, M.F., Marti, O., Merkel, U., Ramstein, G., Valdes, P., Weber, S.L., Yu, Y., Zhao, Y., 2007a. Results of PMIP2 coupled simulations of the mid-Holocene and last glacial maximum—part 1: experiments and large-scale features. Clim. Past 3 (2), 261–277.

Braconnot, P., Otto-Bliesner, B., Harrison, S., Joussaume, S., Peterchmitt, J.Y., Abe-Ouchi, A., Crucifix, M., Driesschaert, E., Fichefet, T., Hewitt, C.D., Kageyama, M., Kitoh, A., Loutre, M.F., Marti, O., Merkel, U., Ramstein, G., Valdes, P., Weber, L., Yu, Y., Zhao, Y., 2007b. Results of PMIP2 coupled simulations of the Mid-Holocene and Last Glacial Maximum—part 2: feedbacks with emphasis on the location of the ITCZ and mid- and high latitudes heat budget. Clim. Past 3 (2), 279–296.

Braun, H., Christl, M., Rahmstorf, S., Ganopolski, A., Mangini, A., Kubatzki, C., Roth, K., Kromer, B., 2005. Solar forcing of abrupt glacial climate change in a coupled climate system model. Nature 438, 208–211.

Broecker, W.S., Andree, M., Bonani, G., Wolfli, W., Oeschger, H., Klas, M., Mix, A., Curry, W., 1988. Preliminary estimates for the radiocarbon age of deep water in the glacial ocean. Paleoceanography 3 (6), 659–669. http://dx.doi.org/10.1029/PA003i006p00659.

Cacho, I., Grimalt, J.O., Pelejero, C., Canals, M., Sierro, F.J., Flores, J.A., Shackleton, N.J., 1999. Dansgaard-Oeschger and Heinrich event imprints in the Alboran Sea paleotemperatures. Paleoceanography 14, 698–705.

Camuffo, D., Sturaro, G., 2003. Sixty-CM submersion of Venice discovered thanks to Canaletto's paintings. Clim. Change 58 (3), 333–343. http://dx.doi.org/10.1023/a:1023902120717.

Carbognin, L., Teatini, P., Tomasin, A., Tosi, L., 2010. Global change and relative sea level rise at Venice: what impact in term of flooding. Clim. Dyn. 35 (6), 1055–1063. http://dx.doi.org/10.1007/s00382-009-0617-5.

Chamberlin, T.C., 1906. On a possible reversal of deep-sea circulation and its influence on geologic climates. J. Geol. 14, 363–373.

Church, J.A., Woodworth, P.L., Aarup, T., Wilson, W., 2010. Understanding Sea-Level Rise and Variability. Blackwell, Oxford.

Clark, P.U., Pisias, N.G., Stocker, T.F., Weaver, A.J., 2002. The role of the thermohaline circulation in abrupt climate change. Nature 415, 863–869.

Clark, P.U., Dyke, A.S., Shakun, J.D., Carlson, A.E., Clark, J., Wohlfarth, B., Mitrovica, J.X., Hostetler, S.W., McCabe, A.M., 2009. The last glacial maximum. Science 325 (5941), 710–714. http://dx.doi.org/10.1126/science.1172873.

Clark, P.U., Shakun, J.D., Baker, P.A., Bartlein, P.J., Brewer, S., Brook, E., Carlson, A.E., Cheng, H., Kaufman, D.S., Liu, Z.Y., Marchitto, T.M., Mix, A.C., Morrill, C., Otto-Bliesner, B.L., Pahnke, K., Russell, J.M., Whitlock, C., Adkins, J.F., Blois, J.L., Clark, J., Colman, S.M., Curry, W.B., Flower, B.P., He, F., Johnson, T.C., Lynch-Stieglitz, J., Markgraf, V., McManus, J., Mitrovica, J.X., Moreno, P.I., Williams, J.W., 2012. Global climate evolution during the last deglaciation. Proc. Natl. Acad. Sci. U.S.A. 109 (19), E1134–E1142. http://dx.doi.org/10.1073/pnas.1116619109.

Claussen, M., et al., 2002. Earth system models of intermediate complexity: closing the gap in the spectrum of climate system models. Clim. Dyn. 18, 579–586.

Cocks, L.R.M., Torsvik, T.H., 2002. Earth geography from 500 to 400 million years ago: a faunal and palaeomagnetic review. J. Geol. Soc. 159, 631–644. http://dx.doi.org/10.1144/0016-764901-118.

Crowley, T.J., Zachos, J.C., 2000. Comparison of zonal temperature profiles for past warm time periods. In: Huber, B.T., MacLeod, K.G., Wing, S.L. (Eds.), Warm Climates in Earth History. Cambridge University Press, Cambridge, UK, pp. 50–76.

Dahl-Jensen, D., Albert, M.R., Aldahan, A., Azuma, N., Balslev-Clausen, D., Baumgartner, M., Berggren, A.M., Bigler, M., Binder, T., Blunier, T., Bourgeois, J.C., Brook, E.J., Buchardt, S.L., Buizert, C., Capron, E., Chappellaz, J., Chung, J., Clausen, H.B., Cvijanovic, I., Davies, S.M., Ditlevsen, P., Eicher, O., Fischer, H., Fisher, D.A., Fleet, L. G., Gfeller, G., Gkinis, V., Gogineni, S., Goto-Azuma, K., Grinsted, A., Gudlaugsdottir, H., Guillevic, M., Hansen, S.B., Hansson, M., Hirabayashi, M., Hong, S., Hur, S.D., Huybrechts, P., Hvidberg, C. S., Iizuka, Y., Jenk, T., Johnsen, S.J., Jones, T.R., Jouzel, J., Karlsson, N.B., Kawamura, K., Keegan, K., Kettner, E., Kipfstuhl, S., Kjaer, H. A., Koutnik, M., Kuramoto, T., Kohler, P., Laepple, T., Landais, A., Langen, P.L., Larsen, L.B., Leuenberger, D., Leuenberger, M., Leuschen, C., Li, J., Lipenkov, V., Martinerie, P., Maselli, O.J., Masson-Delmotte, V., McConnell, J.R., Miller, H., Mini, O., Miyamoto, A., Montagnat-Rentier, M., Mulvaney, R., Muscheler, R., Orsi, A.J., Paden, J., Panton, C., Pattyn, F., Petit, J.R., Pol, K., Popp, T., Possnert, G., Prie, F., Prokopiou, M., Quiquet, A., Rasmussen, S.O., Raynaud, D., Ren, J., Reutenauer, C., Ritz, C., Rockmann, T., Rosen, J.L., Rubino, M., Rybak, O., Samyn, D., Sapart, C.J., Schilt, A., Schmidt, A.M.Z., Schwander, J., Schupbach, S., Seierstad, I., Severinghaus, J.P., Sheldon, S., Simonsen, S.B., Sjolte, J., Solgaard, A.M., Sowers, T., Sperlich, P., Steen-Larsen, H.C., Steffen, K., Steffensen, J.P., Steinhage, D., Stocker, T.F., Stowasser, C., Sturevik, A.S., Sturges, W.T., Sveinbjornsdottir, A., Svensson, A., Tison, J.L., Uetake, J., Vallelonga, P., van de Wal, R.S.W., van der Wel, G., Vaughn, B.H., Vinther, B., Waddington, E., Wegner, A., Weikusat, I., White, J.W.C., Wilhelms, F., Winstrup, M., Witrant, E., Wolff, E.W., Xiao, C., Zheng, J., 2013. Eemian interglacial

reconstructed from a Greenland folded ice core. Nature 493 (7433), 489–494. http://dx.doi.org/10.1038/nature11789.

Deschamps, P., Durand, N., Bard, E., Hamelin, B., Camoin, G., Thomas, A.L., Henderson, G.M., Okuno, J., Yokoyama, Y., 2012. Ice-sheet collapse and sea-level rise at the Bolling warming 14,600 years ago. Nature 483 (7391), 559–564. http://dx.doi.org/10.1038/nature10902.

Deuser, W.G., Hunt, J.M., 1969. Stable isotope ratios of dissolved inorganic carbon in Atlantic. Deep Sea Res. 16 (2), 221–225. http://dx.doi.org/10.1016/0011-7471(69)90078-3.

Donnelly, J.P., Cleary, P., Newby, P., Ettinger, R., 2004. Coupling instrumental and geological records of sea-level change: evidence from southern New England of an increase in the rate of sea-level rise in the late 19th century. Geophys. Res. Lett. 31, L05203. http://dx.doi.org/10.1029/2003gl018933.

Duplessy, J.C., Shackleton, N.J., Matthews, R.K., Prell, W., Ruddiman, W.F., Caralp, M., Hendy, C.H., 1984. C-13 record of benthic foraminifera in the last interglacial ocean—implications for the carbon-cycle and the global deep-water circulation. Quat. Res. 21 (2), 225–243. http://dx.doi.org/10.1016/0033-5894(84)90099-1.

Duplessy, J.-C., Shackleton, N.J., Fairbanks, R.B., Labeyrie, L., Oppo, D., Kallel, N., 1988. Deep water source variations during the last climatic cycle and their impact on the global deep water circulation. Paleoceanography 3, 343–360.

Duplessy, J.C., Labeyrie, L., Waelbroeck, C., 2002. Constraints on the ocean oxygen isotopic enrichment between the last glacial maximum and the Holocene: paleoceanographic implications. Quat. Sci. Rev. 21 (1–3), 315–330. http://dx.doi.org/10.1016/s0277-3791(01)00107-x.

Dutton, A., Lambeck, K., 2012. Ice volume and sea level during the last interglacial. Science 337 (6091), 216–219. http://dx.doi.org/10.1126/science.1205749.

Elderfield, H., Rickaby, R.E.M., 2000. Oceanic Cd/P ratio and nutrient utilization in the glacial Southern ocean. Nature 405 (6784), 305–310. http://dx.doi.org/10.1038/35012507.

Emanuel, K., 2001. Contribution of tropical cyclones to meridional heat transport by the oceans. J. Geophys. Res. 106, 14771–14781. http://dx.doi.org/10.1029/2000JD900641.

Fairbanks, R.G., 1989. A 17,000-year glacio-eustatic sea level record: influence of glacial melting rates on the younger Dryas event and deep-ocean circulation. Nature 342, 637–642.

Fichefet, T., Hovine, S., Duplessy, J.C., 1994. A model study of the Atlantic thermohaline circulation during the last glacial maximum. Nature 372, 252–255.

Gammaitoni, L., Hanggi, P., Jung, P., Marchesoni, F., 1998. Stochastic resonance. Rev. Mod. Phys. 70, 223–287.

Ganopolski, A., Rahmstorf, S., 2001. Rapid changes of glacial climate simulated in a coupled climate model. Nature 409, 153–158.

Ganopolski, A., Rahmstorf, S., 2002. Abrupt glacial climate changes due to stochastic resonance. Phys. Rev. Lett. 88 (3), 038501.

Ganopolski, A., Roche, D.M., 2009. On the nature of lead–lag relationships during glacial–interglacial climate transitions. Quat. Sci. Rev. 28, 3361–3378. http://dx.doi.org/10.1016/j.quascirev.2009.09.019.

Ganopolski, A., Rahmstorf, S., Petoukhov, V., Claussen, M., 1998. Simulation of modern and glacial climates with a coupled global model of intermediate complexity. Nature 391, 351–356.

Ganopolski, A., Calov, R., Claussen, M., 2010. Simulation of the last glacial cycle with a coupled climate ice-sheet model of intermediate complexity. Clim. Past 6 (2), 229–244.

Gehrels, W.R., 1994. Determining relative sea-level change from salt-marsh foraminifera and plant zones on the coast of Maine, USA. J. Coast. Res. 10 (4), 990–1009.

Grinsted, A., Moore, J.C., Jevrejeva, S., 2010. Reconstructing sea level from paleo and projected temperatures 200 to 2100 AD. Clim. Dyn. 34, 461–472. http://dx.doi.org/10.1007/s00382-008-0507-2.

Grootes, P.M., Stuiver, M., White, J.W.C., Johnsen, S., Jouzel, J., 1993. Comparison of oxygen isotope records from the GISP2 and GRIP Greenland ice cores. Nature 366, 552–554.

Hay, W.W., 2008. Evolving ideas about the Cretaceous climate and ocean circulation. Cretaceous Res. 29, 725–753. http://dx.doi.org/10.1016/j.cretres.2008.05.025.

Hay, W.W., Floegel, S., 2012. New thoughts about the Cretaceous climate and oceans. Earth Sci. Rev. 115, 262–272. http://dx.doi.org/10.1016/j.earscirev.2012.09.008.

Hays, J.D., Pitman, W.C., 1973. Lithospheric plate motion, sea level changes and climatic and ecological consequences. Nature 246, 18–22. http://dx.doi.org/10.1038/246018a0.

Hesse, T., Butzin, M., Bickert, T., Lohmann, G., 2011. A model-data comparison of delta C-13 in the glacial Atlantic Ocean. Paleoceanography 26, 16. http://dx.doi.org/10.1029/2010pa002085.

Hofmann, M., Rahmstorf, S., 2009. On the stability of the Atlantic meridional overturning circulation. Proc. Natl. Acad. Sci. U.S.A. 106 (49), 20584–20589. http://dx.doi.org/10.1073/pnas.0909146106.

Hotinski, R.M., Toggweiler, J.R., 2003. Impact of a Tethyan circumglobal passage on ocean heat transport and "equable" climates. Paleoceanography 18, 1007. http://dx.doi.org/10.1029/2001PA000730.

Jevrejeva, S., Grinsted, A., Moore, J.C., Holgate, S., 2006. Nonlinear trends and multiyear cycles in sea level records. J. Geophys. Res. 111, C09012. http://dx.doi.org/10.1029/2005JC003229.

Kageyama, M., Paul, A., Roche, D.M., Van Meerbeeck, C.J., 2010. Modelling glacial climatic millennial-scale variability related to changes in the Atlantic meridional overturning circulation: a review. Quat. Sci. Rev. 29 (21–22), 2931–2956. http://dx.doi.org/10.1016/j.quascirev.2010.05.029.

Kemp, A., Horton, B., Donnelly, J., Mann, M.E., Vermeer, M., Rahmstorf, S., 2011. Climate related sea-level variations over the past two millennia. Proc. Natl. Acad. Sci. U.S.A. 108 (27), 11017–11022. http://dx.doi.org/10.1073/pnas.1015619108.

Kennett, J.P., 1977. Cenozoic evolution of Antarctic glaciation, the circum-Antarctic ocean, and their impact on global paleoceanography. J. Geophys. Res. 82, 3843–3860. http://dx.doi.org/10.1029/JC082i027p03843.

Kim, S.T., O'Neil, J.R., 1997. Equilibrium and non-equilibrium oxygen isotope effects in synthetic carbonates. Geochim. Cosmochim. Acta 61, 3461–3475.

Kopp, R.E., Simons, F.J., Mitrovica, J.X., Maloof, A.C., Oppenheimer, M., 2009. Probabilistic assessment of sea level during the last interglacial stage. Nature 462 (7275), 863–867. http://dx.doi.org/10.1038/nature08686.

Kreveld, S.V., Sarnthein, M., Erlenkeuser, H., Grootes, P., Jung, S., Nadeau, M.J., Pflaumann, U., Voelker, A., 2000. Potential links between surging ice sheets, circulation changes, and the Dansgaard-Oeschger cycles in the Irminger Sea, 60-18 kyr. Paleoceanography 15, 425–442.

Lambeck, K., 2002. Sea-level change from mid-Holocene to recent time: an Australian example with global implications. In: Mitrovica, J.X.,

Vermeersen, L. (Eds.), Glacial Isostatic Adjustment and the Earth System. AGU, Washington, pp. 33–50.

Lambeck, K., Bard, E., 2000. Sea-level change along the French Mediterranean coast for the past 30 000 years. Earth Planet. Sci. Lett. 175 (3–4), 203–222. http://dx.doi.org/10.1016/s0012-821x(99)00289-7.

Lambeck, K., Anzidei, M., Antonioli, F., Benini, A., Espositol, A., 2004. Sea level in Roman times in the central Mediterranean and implications for recent change. Earth Planet. Sci. Lett. 224, 563–575.

Lambeck, K., Woodroffe, C., Antonioli, F., Anzidei, M., Gehrels, W.R., Laborel, J., Wright, A.J., 2010. Paeoenvironmental records, geophysical modeling, and reconstruction of sea-level trends and variability on centennial and longer time scales. In: Church, J.A., Woodworth, P.L., Aarup, T., Wilson, W. (Eds.), Understanding Sea-Level Rise and Variability. Blackwell, Oxford, pp. 61–121.

Lisiecki, L.E., Raymo, M.E., 2005. A Pliocene-Pleistocene stack of 57 globally distributed benthic delta O-18 records. Paleoceanography 20, Pa1003. http://dx.doi.org/10.1029/2004pa001071.

Lyell, C., 1832. Principles of Geology. Murray, London.

Lynch-Stieglitz, J., 2003. Tracers of past ocean circulation. In: Turkekian, K., Holland, H. (Eds.), Treatise on Geochemistry, vol. 6. Elsevier, pp. 433–451.

Lynch-Stieglitz, J., Curry, W.B., Slowey, N., 1999. A geostrophic transport estimate for the Florida current from the oxygen isotope composition of benthic foraminifera. Paleoceanography 14 (3), 360–373. http://dx.doi.org/10.1029/1999pa900001.

Lynch-Stieglitz, J., Adkins, J.F., Curry, W.B., Dokken, T., Hall, I.R., Herguera, J.C., Hirschi, J.J.M., Ivanova, E.V., Kissel, C., Marchal, O., Marchitto, T.M., McCave, I.N., McManus, J.F., Mulitza, S., Ninnemann, U., Peeters, F., Yu, E.F., Zahn, R., 2007. Atlantic meridional overturning circulation during the last glacial maximum. Science 316 (5821), 66–69. http://dx.doi.org/10.1126/science.1137127.

Lynch-Stieglitz, J., Curry, W.B., Lund, D.C., 2009. Florida Straits density structure and transport over the last 8000 years. Paleoceanography 24, 9. http://dx.doi.org/10.1029/2008pa001717.

Margari, V., Skinner, L.C., Tzedakis, P.C., Ganopolski, A., Vautravers, M., Shackleton, N.J., 2010. The nature of millennial-scale climate variability during the past two glacial periods. Nat. Geosci. 3 (2), 127–131. http://dx.doi.org/10.1038/ngeo740.

McCulloch, M.T., Tudhope, A.W., Esat, T.M., Mortimer, G.E., Chappell, J., Pillans, B., Chivas, A.R., Omura, A., 1999. Coral record of equatorial sea-surface temperatures during the penultimate deglaciation at Huon Peninsula. Science 283 (5399), 202–204. http://dx.doi.org/10.1126/science.283.5399.202.

McKay, N.P., Overpeck, J.T., Otto-Bliesner, B.L., 2012. The role of ocean thermal expansion in last interglacial sea level rise. Geophys. Res. Lett. 38, L14605. http://dx.doi.org/10.1029/2011gl048280.

Milankovitch, M., 1941. Kanon der Erdbestrahlung und seine Anwendung auf das Eiszeitenproblem. Königlich Serbische Akademie, Belgrad.

Miller, K.G., Kominz, M.A., Browning, J.V., Wright, J.D., Mountain, G.S., Katz, M.E., Sugarman, P.J., Cramer, B.S., Christie-Blick, N., Pekar, S.F., 2005. The phanerozoic record of global sea-level change. Science 310, 1293–1298. http://dx.doi.org/10.1126/science.1116412.

Müller, R.D., Sdrolias, M., Gaina, C., Roest, W.R., 2008a. Age, spreading rates, and spreading asymmetry of the world's ocean crust. Geochem. Geophys. Geosyst. 9, Q04006. http://dx.doi.org/10.1029/2007GC001743.

Müller, R.D., Sdrolias, M., Gaina, C., Steinberger, B., Heine, C., 2008b. Long-term sea-level fluctuations driven by ocean basin dynamics. Science 319, 1357–1362. http://dx.doi.org/10.1126/science.1151540.

Negre, C., Zahn, R., Thomas, A.L., Masque, P., Henderson, G.M., Martinez-Mendez, G., Hall, I.R., Mas, J.L., 2010. Reversed flow of Atlantic deep water during the last glacial maximum. Nature 468 (7320), 84. http://dx.doi.org/10.1038/nature09508.

Oppo, D., Lehman, S.J., 1993. Mid-depth circulation of the subpolar North Atlantic during the last glacial maximum. Science 259, 1148–1152.

Ota, Y., Chappell, J., 1999. Holocene sea-level rise and coral reef growth on a tectonically rising coast, Huon Peninsula, Papua New Guinea. Quat. Int. 55, 51–59. http://dx.doi.org/10.1016/s1040-6182(98)00024-x.

Otto-Bliesner, B.L., Brady, E.C., 2010. The sensitivity of the climate response to the magnitude and location of freshwater forcing: last glacial maximum experiments. Quat. Sci. Rev. 29 (1–2), 56–73. http://dx.doi.org/10.1016/j.quascirev.2009.07.004.

Otto-Bliesner, B.L., Upchurch Jr., G.R., 1997. Vegetation-induced warming of high-latitude regions during the late Cretaceous period. Nature 385, 804–807.

Passaro, S., Barra, M., Saggiomo, R., Di Giacomo, S., Leotta, A., Uhlen, H., Mazzola, S., 2013. Multi-resolution morpho-bathymetric survey results at the Pozzuoli-Baia underwater archaeological site (Naples, Italy). J. Archaeol. Sci. 40 (2), 1268–1278. http://dx.doi.org/10.1016/j.jas.2012.09.035.

Pearson, P.N., Ditchfield, P.W., Singano, J., Harcourt-Brown, K.G., Nicholas, C.J., Olsson, R.K., Shackleton, N.J., Hall, M.A., 2001. Warm tropical sea surface temperatures in the late Cretaceous and Eocene epochs. Nature 413, 481–487. http://dx.doi.org/10.1038/413481A0.

Peltier, W.R., Fairbanks, R.G., 2006. Global glacial ice volume and last glacial maximum duration from an extended Barbados sea level record. Quat. Sci. Rev. 25 (23–24), 3322–3337. http://dx.doi.org/10.1016/j.quascirev.2006.04.010.

Pirazzoli, P.A., Evelpidou, N., 2013. Tidal notches: a sea-level indicator of uncertain archival trustworthiness. Palaeogeogr. Palaeoclimatol. Palaeoecol. 369, 377–384. http://dx.doi.org/10.1016/j.palaeo.2012.11.004.

Rahmstorf, S., 2002. Ocean circulation and climate during the past 120,000 years. Nature 419, 207–214.

Rahmstorf, S., 2003. Timing of abrupt climate change: a precise clock. Geophys. Res. Lett. 30, 1510.

Rahmstorf, S., 2007. A semi-empirical approach to projecting future sea-level rise. Science 315 (5810), 368–370.

Robinson, A., Calov, R., Ganopolski, A., 2011. Greenland ice sheet model parameters constrained using simulations of the Eemian Interglacial. Clim. Past 7 (2), 381–396. http://dx.doi.org/10.5194/cp-7-381-2011.

Robinson, A., Calov, R., Ganopolski, A., 2012. Multistability and critical thresholds of the Greenland ice sheet. Nat. Clim. Chang. 2 (6), 429–432. http://dx.doi.org/10.1038/nclimate1449.

Rohling, E.J., Fenton, M., Jorissen, F.J., Bertrand, P., Ganssen, G., Caulet, J.P., 1998. Magnitudes of sea-level lowstands of the past 500,000 years. Nature 394, 162–165. http://dx.doi.org/10.1038/28134.

Rose, B.E.J., Ferreira, D., 2013. Ocean heat transport and water vapor greenhouse in a warm equable climate: a new look at the low gradient

paradox. J. Clim. 26, 2117–2136. http://dx.doi.org/10.1175/JCLI-D-11-00547.1.

Rosenthal, Y., Boyle, E.A., Slowey, N., 1997. Temperature control on the incorporation of magnesium, strontium, fluorine, and cadmium into benthic foraminiferal shells from Little Bahama Bank: prospects for thermocline paleoceanography. Geochim. Cosmochim. Acta 61 (17), 3633–3643. http://dx.doi.org/10.1016/s0016-7037(97)00181-6.

Royer, D.L., 2006. CO2-forced climate thresholds during the Phanerozoic. Geochim. Cosmochim. Acta 70, 5665–5675. http://dx.doi.org/10.1016/j.gca.2005.11.031.

Ruddiman, W.F., 2000. Earths Climate: Past and Future. Freeman, New York, p. 465.

Rutberg, R.L., Hemming, S.R., Goldstein, S.L., 2000. Reduced North Atlantic deep water flux to the glacial Southern ocean inferred from neodymium isotope ratios. Nature 405 (6789), 935–938.

Sachs, J.P., Lehman, S.J., 1999. Subtropical North Atlantic temperatures 60,000 to 30,000 years ago. Science 286, 756–759.

Sarnthein, M., Winn, K., Jung, S.J.A., Duplessy, J.C., Labeyrie, L., Erlenkeuser, H., Ganssen, G., 1994. Changes in east Atlantic deep-water circulation over the last 30,000 years: eight time slice reconstructions. Paleoceanography 9, 209–267.

Schmidt, G.A., 1999. Forward modeling of carbonate proxy data from planktonic foraminifera using oxygen isotope tracers in a global ocean model. Paleoceanography 14 (4), 482–497. http://dx.doi.org/10.1029/1999pa900025.

Schrag, D.P., Adkins, J.F., McIntyre, K., Alexander, J.L., Hodell, D.A., Charles, C.D., McManus, J.F., 2002. The oxygen isotopic composition of seawater during the last glacial maximum. Quat. Sci. Rev. 21 (1–3), 331–342. http://dx.doi.org/10.1016/s0277-3791(01)00110-x.

Schulz, M., 2002. On the 1470-year pacing of Dansgaard-Oeschger warm events. Paleoceanography 17, 4-1–4-9.

Scott, D.S., Medioli, F.S., 1978. Vertical zonations of Marsh foraminifera as accurate indicators of former sea-levels. Nature 272 (5653), 528–531. http://dx.doi.org/10.1038/272528a0.

Sewall, J.O., van de Wal, R.S.W., van der Zwan, K., van Oosterhout, C., Dijkstra, H.A., Scotese, C.R., 2007. Climate model boundary conditions for four Cretaceous time slices. Clim. Past 3, 647–657. http://dx.doi.org/10.5194/cp-3-647-2007.

Shackleton, N.J., 2000. The 100,000-year ice-age cycle identified and found to lag temperature, carbon dioxide, and orbital eccentricity. Science 289, 1897–1902. http://dx.doi.org/10.1126/science.289.5486.1897.

Shennan, I., et al., 2007. Sea level studies. In: In: Elias, S.A. (Ed.), Encyclopedia of Quaternary Science, vol. 4. Elsevier, Amsterdam, pp. 2967–3095.

Sivan, D., Lambeck, K., Toueg, R., Raban, A., Porath, Y., Shirman, B., 2004. Ancient coastal wells of Caesarea Maritima, Israel, an indicator for relative sea level changes during the last 2000 years. Earth Planet. Sci. Lett. 222 (1), 315–330. http://dx.doi.org/10.1016/j.epsl.2004.02.007.

Spero, H.J., Lea, D.W., 1996. Experimental determination of stable isotope variability in Globigerina bulloides: implications for paleoceanographic reconstructions. Mar. Micropaleontol. 28 (3–4), 231–246. http://dx.doi.org/10.1016/0377-8398(96)00003-5.

Stanford, J.D., Rohling, E.J., Hunter, S.E., Roberts, A.P., Rasmussen, S.O., Bard, E., McManus, J., Fairbanks, R.G., 2006. Timing of meltwater pulse 1a and climate responses to meltwater injections. Paleoceanography 21, Pa4103. http://dx.doi.org/10.1029/2006pa001340.

Stanley, S., 2005. Earth System History. W.H. Freeman, New York, p. 567.

Stocker, T.F., 1998. The seesaw effect. Science 282, 61–62.

Stocker, T.F., Johnsen, S.J., 2003. A minimum thermodynamic model for the bipolar seesaw. Paleoceanography 18, art. no. 1087 http://onlinelibrary.wiley.com/http://dx.doi.org/10.1029/2003PA000920/abstract.

Stuiver, M., Quay, P.D., Ostlund, H.G., 1983. Abyssal water C-14 distribution and the age of the world oceans. Science 219 (4586), 849–851. http://dx.doi.org/10.1126/science.219.4586.849.

Tachikawa, K., Elderfield, H., 2002. Microhabitat effects on Cd/Ca and delta C-13 of benthic foraminifera. Earth Planet. Sci. Lett. 202 (3–4), 607–624. http://dx.doi.org/10.1016/s0012-821x(02)00796-3.

Torsvik, T.H., Cocks, L.R.M., 2004. Earth geography from 400 to 250 Ma: a palaeomagnetic, faunal and facies review. J. Geol. Soc. 161, 555–572. http://dx.doi.org/10.1144/0016-764903-098.

Turney, C.S.M., Jones, R.T., 2010. Does the Agulhas current amplify global temperatures during super-interglacials? J. Quat. Sci. 25 (6), 839–843. http://dx.doi.org/10.1002/jqs.1423.

Waelbroeck, C., Labeyrie, L., Michel, E., Duplessy, J.C., McManus, J.F., Lambeck, K., Balbon, E., Labracherie, M., 2002. Sea-level and deep water temperature changes derived from benthic foraminifera isotopic records. Quat. Sci. Rev. 21 (1–3), 295–305.

Weber, S.L., Drijfhout, S.S., Abe-Ouchi, A., Crucifix, M., Eby, M., Ganopolski, A., Murakami, S., Otto-Bliesner, B., Peltier, W.R., 2007. The modern and glacial overturning circulation in the Atlantic Ocean in PMIP coupled model simulations. Clim. Past 3 (1), 51–64.

Wefer, G., Berger, W.H., 1991. Isotope paleontology—growth and composition of extant Calcareous species. Mar. Geol. 100 (1–4), 207–248. http://dx.doi.org/10.1016/0025-3227(91)90234-u.

Woodroffe, C., McLean, R., 1990. Microatolls and recent sea-level change on coral atolls. Nature 344 (6266), 531–534. http://dx.doi.org/10.1038/344531a0.

Yu, E.-F., Francois, R., Bacon, M.P., 1996. Similar rates of modern and last-glacial ocean thermohaline circulation inferred from radiochemical data. Nature 379, 689–694.

Zhou, J., Poulsen, C.J., Rosenbloom, N., Shields, C., Briegleb, B., 2012. Vegetation-climate interactions in the warm mid-Cretaceous. Clim. Past 8, 565–576. http://dx.doi.org/10.5194/cp-8-565-2012.